Projection, Spatial Correlations, and Anisotropies in a Large and Complete Sample of Abell Clusters

Christopher J. Miller, David J. Batuski, Kurt A. Slinglend
Department of Physics and Astronomy, University of Maine, Orono ME 04469-5709

and

John. M. Hill
Steward Observatory, University of Arizona, Tucson AZ 85721-0065

ABSTRACT

An analysis of $R \geq 1$ Abell clusters is presented for samples containing recent redshifts from the MX Northern Abell Cluster Survey. The newly obtained redshifts from the MX Survey as well as those from the ESO Nearby Abell Cluster Survey (ENACS) provide the necessary data for the largest magnitude-limited correlation analysis of rich clusters in the entire sky (excluding the galactic plane) to date. The MX Survey, undertaken primarily for large-scale structure studies, has provided a large compilation of galaxy redshifts in Abell cluster fields for the examination of projection effects within the Abell catalog. In addition, a large and complete set of cluster velocities (to $m_{10} = 16.8$) is used to determine the two-point spatial correlation function and examine previously suggested line-of-sight cluster selection bias within the Abell catalog.

The two-point spatial correlation function is determined for a complete magnitude-limited ($m_{10} \leq 16.8$) sample of northern Abell clusters ($N_{cl} = 198$), a complete whole-sky (excluding the galactic plane) magnitude-limited ($m_{10} \leq 16.8$) sample of Abell/ACO clusters ($N_{cl} = 289$), and a complete whole-sky magnitude and volume-limited ($m_{10} \leq 16.8$, $z \leq 0.1$) sample of Abell/ACO clusters ($N_{cl} = 238$) In addition, we examined the largest sample of cD clusters ($N_{cl} = 104$) in the Northern hemisphere. We find $19.4 \leq r_0 \leq 23.3h^{-1}$Mpc, $-1.92 \leq \gamma \leq -1.83$ for the different cluster subsets examined (including the cD clusters).

We have used the largest rich cluster data set available to date to look for line-of-sight anisotropies within the Abell/ACO catalogs. An examination of the correlation function separated into its line-of-sight and perpendicular-to-line-of-sight components show that the strong anisotropy present in previously

studied Abell cluster datasets is not present in our samples. There are, however, indications of residual anisotropies which we show are the result of two elongated superclusters, Ursa Majoris and Corona Borealis whose axes lie near the line-of-sight. After rotating these superclusters so that their semi-major axes are perpendicular to the line-of-sight, we find no indication of anisotropy in $\xi(\sigma, \pi)$. The amplitude and slope of the correlation function remain the same before and after these rotations. We also remove a subset of $R = 1$ Abell/ACO clusters that show sizeable foreground/background galaxy contamination and again find no change in the amplitude or slope of the correlation function. We conclude that the correlation length of $R \geq 1$ Abell clusters is not artificially enhanced by line-of-sight anisotropies.

1. Introduction

The study of large-scale structure in the Universe plays a vital role in the determination of the cosmological parameters and scenarios that describe the Universe from just after its creation to what we see today. It is the visible structure on scales greater than $\sim 50h^{-1}$Mpc (where h is the Hubble constant in units of 100 km s^{-1} Mpc^{-1}) that can tell us directly about the nature of the initial conditions which could have generated such structures. Most researchers believe that low amplitude Gaussian density perturbations, resulting from quantum fluctuations in the earliest stages of cosmic evolution, seeded the large-scale structure we see today (Guth & Pi 1982; Linde 1982; Bardeen, Steinhardt & Turner 1983). (Although non-Gaussian initial conditions have been suggested, including topological defects (Zeldovich 1980; Vilenkin 1981) and global structures (Turok 1989).)

While the data still remain sparse, there have been a variety of tracers used successfully for observing large-scale structure through redshift studies: individual galaxies in wide-area magnitude-limited and pencil-beam surveys, visually-selected galaxy clusters, plate-scanned clusters, X-ray-selected clusters, groups of galaxies, and cD clusters. On the largest of scales, galaxy clusters are more efficient tracers than individual galaxies. While galaxy surveys such as the Sloan Digital Sky Survey (SDSS) and the Australian 2dF Survey will undoubtedly yield excellent datasets for structure analyses, current surveys such as the CfA (Geller & Huchra, 1989) and the Las Campanas Survey (Shectman et al. 1996) among others, lack the depth, volume and completeness of coverage needed for accurate evaluations of the two-point correlation function, power spectrum, and other measures of structure on scales of $100h^{-1}$Mpc and greater. As of the writing of this paper, both the SDSS and the 2dF surveys are years from completion and public access to the data.

X-ray-selected cluster catalogs avoid visual selection or projection biases. The thermal X-ray emission from intracluster gas confined to the gravitational potential wells of galaxy clusters is typically bright and highly peaked at the gravitational center of the clusters. The ROSAT Brightest Cluster Sample (BCS) is a 90% complete, flux limited sample of 199 X-ray brightest clusters in the Northern Hemisphere that has provided a detailed evaluation of the X-ray luminosity function (XLF) out to a redshift $z \leq 0.3$ (Ebeling, *et al.* 1997). This new survey may provide an excellent sample for large-scale structure studies and for comparison with optically identified clusters. However, there are questions as to exactly what type of clusters (specifically in richness and shape) the X-ray samples trace. Bahcall & Cen (1994) show that flux-limited X-ray samples contain poor nearby clusters and rich distant clusters. A flux-limited sample of clusters would contain a mixture of rich and poor clusters, both of which could be incomplete in regions of the observed volume. Struble & Ftaclas (1994) indicate that rich clusters are intrinsically more nearly spherical than poor

$R = 0$ clusters. A preferable sample would contain the same type of cluster (i.e. clusters with similar properties in shape and membership), showing a constant average density in a large volume of space.

The first northern sky catalog of rich galaxy clusters was created by George Abell in 1958 from visually scanned sky survey plates. Abell's (1958) $R \geq 1$ clusters are ideally rare for large-scale structure studies. They have an average spatial separation of $\sim 50h^{-1}$ Mpc, making them very efficient samplers of the mass distribution on scales larger than 100 h^{-1} Mpc. A minimum of telescope time is required to map such large scales with clusters, since spectroscopy of only a few relatively bright galaxies is needed to obtain a reliable redshift for a cluster. For the above reasons, we have chosen the $R \geq 1$ Abell clusters as our sparse tracers, assuming that they represent the underlying mass distribution.

In the Northern Hemisphere, several researchers have used optically-observed rich galaxy clusters to trace large-scale structure (for example, Bahcall & Soneira 1983, Batuski & Burns 1985 and Postman, Huchra, & Geller 1992). These efforts provide evidence for a strong signal of structure on scales $> 50h^{-1}$ Mpc. However, the samples utilized by these authors suffer from two limitations: small sample size and single redshifts for many clusters. These limitations impose lower confidence in any of the statistical analyses performed. Prior to the MX Northern Abell Cluster Survey, the complete, magnitude-limited sample of Abell cluster redshifts extended only to $m_{10} \leq 16.5$, where m_{10} is the apparent magnitude (photored) of the tenth brightest galaxy within the cluster. This sample, presented by Postman, Huchra and Geller (1992, hereafter PHG) consisted of 156 $R \geq 1$ Abell clusters with $\delta \geq -27.5°$. When a galactic latitude limit of $|b| \geq 30°$ is applied, 126 clusters remain in the sample. Of these 126, 35 cluster velocities were determined by measuring the redshift of a single galaxy within the respective cluster, resulting in unreasonably large uncertainty in the velocities due to projection. The small fraction of $R \geq 1$ clusters with observed redshifts, and even smaller fraction with multiple-galaxy-determined redshifts, has resulted in a severely limited sample for large-scale structure studies.

The MX Northern Abell Cluster Survey was undertaken in an attempt to rectify these two incompleteness problems associated with the Abell sample of clusters: the small number of clusters with multiple-galaxy observed redshifts (that comprise a complete sample) and projection effects on cluster membership. The MX Survey has increased the latitude-limited, magnitude-limited sample size to 198 $R \geq 1$ clusters (98% complete to $m_{10} \leq 16.8$). At the same time, we have reduced cluster redshift uncertainties, since 187 of these clusters now have more than one measured cluster member redshift. Slinglend *et al.* (1998) have obtained an average of nine cluster member redshifts in 88 observed clusters. The MX Survey has provided a substantially enlarged dataset of $R \geq 1$ Abell clusters for

the analyses in this paper. We remind the reader that the $R = 0$ subset of Abell clusters does not comprise a statistically complete sample. The $R = 0$ clusters were included in the Abell catalog only to enhance its value as a cluster finding list (Abell 1958; Struble & Rood 1991), not for use in spatial analyses.

The Abell and Abell, Corwin, and Olowin (1989-hereafter ACO) catalogs are the only optical cluster catalogs available that cover the entire sky. The volume of space that is spatially analyzed in this paper is the largest to date. If structures exist on scales greater than $50h^{-1}$Mpc, any statistical analysis must use volumes of space substantially larger than the size of the largest features. Smaller surveys, such as all current galaxy surveys, pencil-beam surveys and the plate-scanned cluster surveys (*e.g.* APM) are only marginally large enough to detect very large-scale structure. While the potential of the Abell/ACO catalogs is obvious, their utility has come under question due to anisotropies detected within the catalogs (Sutherland 1988; Efstathiou *et al.* 1992; Dalton *et al.* 1994; Peacock & West 1992). The analyses used in describing these anisotropies indicate that Abell (1958) preferentially cataloged clusters near the lines-of-sight towards other clusters. Unfortunately, the samples used for these analyses are themselves small and incomplete. Incomplete datasets used in large-scale structure analyses are subject to observational bias. The Sutherland and Peacock & West anisotropy analyses used highly incomplete samples. The PHG statistical sample of 208 $R \geq 0$ Abell clusters (used by Efstathiou *et al.* to show anisotropy within the catalog) is only compete to $m_{10} = 16.5$ and contains over 100 $R = 0$ clusters. While there have been a number of papers suggesting that the anisotropy is actually the result of high peculiar velocities, the elongation of cluster pairs in the redshift direction, real geometric elongation of superclusters, or some combination of these, none has offered definitive observational evidence (Jing *et al.* 1992; Bahcall *et al.* 1986).

The aim of this paper is to show that the Abell/ACO $R \geq 1$ clusters form a large and complete dataset with minimal projection effects and line-of-sight anisotropies. The amplitude and slope of the two-point spatial correlation function are re-examined using the largest (in number and in volume) $R \geq 1$ clusters sample to date. In Section 2 projection effects are examined, Section 3 defines some independent and partially independent samples within the entire dataset for analysis, and Section 4 covers the determination of the mean space density of rich clusters. In Section 5 we present the cluster-cluster spatial correlation function for the subsamples of clusters. Section 6 discusses the analysis of anisotropies in the Abell catalog, and our results are summarized in Section 7.

2. Projection effects

In past large-scale structure analyses (using clusters), many of the cluster distances were determined by the observation of a single galaxy member (Bahcall & Soneira 1983; PHG). To examine the uncertainty inherent in using clusters with only one measured redshift, we calculated velocity differences for cluster redshifts published in PHG and Quintana & Ramirez (1995) when compared to the MX Survey redshifts of Slinglend *et al.* (1998). We used 36 clusters within $z \leq 0.13$, all of which had only one measured galaxy before the MX Survey and which now have an average of nine galaxy redshifts of cluster members. Figure 1 shows these velocity differences as a function of redshift. A0121 and A0769 show the most extreme differences of ~ 14000 km s^{-1} and ~ 6000 km s^{-1} respectively. Five of the thirty-six clusters studied have velocity differences of ~ 2000 km s^{-1} or greater, while thirteen differ by ~ 500 km s^{-1}. We conclude that projected membership (or at least extreme outliers in the velocity distribution of clusters) was a problem for 14% of the previously single-measurement clusters. The velocity errors of ~ 500 km s^{-1} for the second category of deviations (in 36% of the clusters) are the result of typical velocity dispersions within Abell clusters which could impact the structure signal on smaller scales ($\sim 5h^{-1}$Mpc). However, the peculiar velocities of clusters have been shown to be ~ 500 km s^{-1} (Bahcall & Oh 1996), so the use of the Hubble flow to study relative cluster positions on such small scales is inappropriate in any case. Nevertheless, the results for the clusters in the higher deviation category indicate that projection (or selection of a galaxy in the wings of the cluster velocity distribution) can be problematic when using a sample that has a substantial number of cluster redshifts based on a single measurement.

Another concern of clusters in the Abell catalog is the misclassification of richness levels. There have been claims that projection effects on cluster richness designations is a serious problem in the Abell catalog (*e.g.* Lucey *et al.* 1983). Recently however, two of the most extensive rich cluster surveys, the MX Survey (Slinglend *et al.* 1998) and the ENACS survey (Katgert *et al.* 1996), find only $\sim 10\%$ of clusters to have more than $\sim 30\%$ of galaxies per cluster field to be foreground/background. Abell (1958) in fact, claimed that up to 30% of the galaxies within a cluster field were background/foreground galaxies. After subtracting a locally estimated background count, Abell determined the total number of galaxies within each cluster to his specified magnitude limit. Clusters containing 30-49 galaxies were classified as $R = 0$, clusters containing 50-79 galaxies were classified as $R = 1$, and so on. The difficulty for Abell was twofold: (1) not knowing the redshifts of any of the galaxies in fields he was examining and (2) having to estimate the redshifts of clusters as well as their linear diameters on the sky (corresponding to $1.5h^{-1}$Mpc). Difficulty (1) was addressed by subtracting the background galaxy count (derived from a nearby region on the plate apparently 'free' of clusters). Difficulty (2) was handled by using an $m_{10} - z$ relation

derived from 18 clusters with known redshifts (in 1958). The 22 galaxies (on average) per cluster field observed by the MX Survey provides an excellent database for comparing the true background fraction with that estimated by Abell. In addition, we can examine how many clusters had underestimated (or overestimated) angular diameters which would affect their richness assignment. We note that the MX Survey has not provided enough galaxy redshifts for a determination of the absolute cluster membership of Abell clusters.

We examined galaxies within one Abell radius of the cluster center as defined using an $m_{10} - z$ derived from Abell (1958). The estimator is

$$log(cz) = 0.71 + 0.23 m_{10}. \quad (1)$$

We first look at those clusters for which the actual redshift and the estimated redshift differ by less than 4000 km s^{-1}, *i.e.* where Abell's distance estimate was 'correct'. There are 29/80 such cases and we find that 27% of the galaxies observed in these fields were foreground/background. Therefore, when Abell's redshift estimate was near the true redshift of the cluster, subtracting up to $\sim 30\%$ of the galaxy count due to foreground/background contamination is appropriate. For the remaining clusters, we find that the majority of the cluster redshifts (44/80) are over-estimated using equation (1), resulting in a much smaller effective radius within which galaxies were counted. Since most Abell clusters have well-defined cores, we expect the fraction of foreground/background galaxies to be lower for these cases. In fact, we find only 20% contamination when the estimated cluster redshift is much greater ($> +4000$ km s^{-1}) than the true redshift. According to Abell (1958), altering the angular diameter corresponding to one Abell radius ($1.5h^{-1}$Mpc) by $\pm 30\%$ would not affect the richness classification. However, we find that 37 of the 44 clusters with overestimated redshifts have angular diameters (corresponding to one Abell radius) on the sky which are more than 30% larger than that used by Abell. Therefore, 91% of the clusters in this analysis ($m_{10} \leq 16.8, R \geq 1$) would have the same or greater richness classification had their true redshifts been used. Only 7/80 clusters have underestimated redshifts according to equation (1) . These results do not change significantly ($1 - 3\%$) when using Abell radii up to 2.5 h^{-1}Mpc.

The MX Survey has provided too few galaxy redshifts per cluster field for an accurate galaxy-member count. However, by examining the true redshifts of the clusters and their foreground/background galaxy fractions, we can conclude that the apparent richnesses, as classified by Abell (1958), are generally accurate (or perhaps underestimated). Since the remaining analyses in this paper are based on $R \geq 1$ clusters, underestimated richness levels would not alter any of the results.

3. The Cluster Samples

The addition of the MX Survey clusters to ones previously measured by other researchers (PHG, Struble & Rood 1987) brings the total number of observed clusters with $m_{10} \leq 16.8$, $R \geq 1$, $-17^\circ \leq \delta \leq 90^\circ$ to 193 (out of 198 listed in the Abell (1958) catalog). A recent survey in the southern hemisphere, the ESO Nearby Abell Cluster Survey (ENACS) has added redshifts for 104 $R \geq 1$ ACO clusters with mean redshifts $z \leq 0.1$ (Katgert *et al.* 1996). The depth of the ENACS survey is similar to the MX survey and thus provides an excellent southern dataset that can be combined with the MX survey for all-sky studies. We note that there are differences between $R \geq 1$ Abell clusters and $R \geq 1$ ACO clusters (*e.g.* Batuski *et al.* 1989 and references therein). Such differences between the catalogs include: V *vs.* R band magnitude determinations (ACO and Abell respectively), greater sensitivity of the IIIa-J plates used in the ACO catalog, and a global determination of the background galaxy count vs. local determinations (ACO and Abell respectively). For the correlation analyses presented in this paper we will be examining four different subsets of clusters summarized below.

1. **The northern magnitude-limited sample** is the 198 Abell $m_{10} \leq 16.8$, R≥ 1 clusters with $0^h \leq \alpha \leq 24^h$, $-17^\circ \leq \delta \leq 90^\circ$, and $|b| \geq 30^\circ$. Five of these clusters have estimated redshifts from the Batuski & Burns (1985) magnitude-redshift relation.

2. **The whole-sky magnitude-limited sample** contains the 198 Abell $m_{10} \leq 16.8$, R≥ 1 clusters in the above northern sample plus 91 $R \geq 1$, $m_{10} \leq 16.8$, ACO clusters with $-90^\circ \leq \delta \leq -17^\circ$, $0^h \leq \alpha \leq 24^h$. Six of the ACO clusters have estimated redshifts according to the $m_{10} - z$ relations in the ACO the catalog. In section 4, we find a higher mean density for the ACO sample of clusters compared to the Abell sample, supporting previous claims that the ACO clusters are slightly poorer than their northern counterparts. Therefore, to create a homogeneous sample containing both ACO and Abell clusters (to similar richness), we have excluded the 14 poorest ACO $R = 1$ clusters (those with $N_{gal} \leq 54$ where N_{gal} is the number of galaxies within an Abell radius as listed in the ACO catalog). The remaining sample of 91 ACO clusters has a mean spatial number density similar to that of the Abell clusters (see section 4). This sample is the largest $R \geq 1$ cluster sample to date and contains 289 clusters.

3. **The whole-sky statistical sample** is a subset of the previous sample excluding any clusters that lie beyond $z = 0.10$. The northern Abell cluster magnitude and volume-limited sample contains 156 clusters (two with estimated redshifts). The

Southern hemisphere magnitude and volume-limited sample contains 82 ACO clusters (five with estimated redshifts).

4. **The volume-limited cD sample** contains cD clusters as defined in ACO (1989). This sample is volume-limited to $D \leq 350$ h^{-1}Mpc, and $0^h \leq \alpha \leq 24^h$, $-17° \leq \delta \leq 90°$, and $|b| \leq 30°$. We apply no richness constraint to this sample of 104 clusters. A smaller sample of cD clusters ($N_{cl} = 64$) was previously used for large-scale structure analyses in West & van den Bergh (1991). Schombert & West (1990) have shown that cD clusters have a distribution representative of Abell clusters in general. Thus by limiting a sample to only cD clusters, we should not be introducing any additional biases. This sample is somewhat independent from the others, since it has different selection criteria and contains a substantial number of $R = 0$ clusters.

Distances to all clusters were determined from Sandage (1975) where

$$D = \frac{cz}{H_o} \frac{(1 + \frac{z}{2})}{(1 + z)} \tag{2}$$

for a Friedman universe with $q_0 = 0$. All of the samples have an additional constraint of $|b| \geq 30°$, to limit the effects of galactic obscuration near the plane of the Galaxy. Figure 2 shows Aitoff projections for the northern magnitude-limited sample and the whole-sky magnitude-limited sample (in galactic coordinates).

The number of clusters within the whole-sky sample makes it the largest set of $R \geq 1$ Abell clusters that has yet been used for correlation analyses. In addition, the volume traced by these clusters ($\sim 5 \times 10^7 h^{-3}$Mpc^3) is the largest using a complete sample. Together, the large number of clusters and volume of space studied in the following analyses provide a most complete picture of large-scale structure in the local Universe.

4. The Spatial Number Density of Clusters

The number density in a proper volume, $n_p(z)$, of a survey can be calculated for a Friedmann Universe (Narlikar 1983) :

$$dn_o = d\Omega (\frac{c}{H_o})^3 \frac{\{q_0 z + (q_0 - 1)[(1 + 2zq_0)^{1/2} - 1]\}^2 n_p dz}{q_0^4 (1 + z)^6 (1 + 2q_0 z)^{1/2}}, \tag{3}$$

and we have

$$dn_o = d\Omega (\frac{c}{H_o})^3 \frac{z^2 (2 + z)^2 n_p dz}{4(1 + z)^6} \tag{4}$$

for $q_0 = 0$, where dn_o is the number of observed clusters within dz and $d\Omega$ is the solid angle subtended by the survey.

If we include an unknown selection function in z, $S(z)$, and the evolution of n_p via $E(z)$, we must let $n_p(z) \rightarrow n_p(z)S(z)E(z)$ (Kolb & Turner 1990). For the samples mentioned above, we assume $E(z) = S(z) = 1$ for simplicity, since evolution of the proper number density of clusters should be negligible at these low redshifts and we are only studying a volume that has a nearly constant density (see Figure 3), making S(z) ~ 1. Figure 3 shows the number density (n_p) as a function of z for the northern magnitude-limited sample and the southern magnitude-limited sample.

The solid angle of the sky covered by the MX Northern sample of 198 clusters is 4.25 steradians. The whole-sky magnitude-limited sample of 282 clusters covers an area of 6.28 steradians (the entire sky excluding galactic latitudes below 30°.) Using Figure 3, we see the number density no longer being constant at $z = 0.09$. Averaging the weighted mean number densities in Figures 3a,b (to $z = 0.09$) we find $\bar{n}_p = 6.6(\pm 0.6) \times 10^{-6} h^3 \mathrm{Mpc}^{-3}$ for the northern Abell clusters and $\bar{n}_p = 7.6(\pm 0.9) \times 10^{-6} h^3 \mathrm{Mpc}^{-3}$ for the southern ACO clusters (using 1σ errors). To create the whole-sky clusters sample, we excluded 14 ACO clusters (those with $N_{gal} \leq 54$), reducing the density for the ACO sample to $\bar{n}_p = 6.5(\pm 0.9) \times 10^{-6} h^3 \mathrm{Mpc}^{-3}$. [The MX Survey II is nearing completion after observing most Abell clusters with $16.9 \leq m_{10} \leq 17.0$ (Miller *et al.* 1999). The additional ~ 100 clusters provided by the MX Survey II should increase the density slightly more, as a few low redshift clusters are added. With the results from the MX Survey II, we expect to have a sample deep enough in magnitude to calculate an accurate density for a volume-limited sample of clusters to $z = 0.10$.]

The number density for the northern clusters implies a mean separation length of $\sim 50 h^{-1}$Mpc. For comparison, the spatial number density of APM clusters is three times as large at $\sim 2.4 \times 10^{-5} h^3 \mathrm{Mpc}^{-3}$. APM clusters are thus even less rich than $R = 0$ Abell clusters and therefore much less rare (Bahcall & West 1992). Our redshift limit of $z = 0.10$ for the magnitude and volume-limited samples (discussed in Section 3) was based on the redshift where n_p differs from $\bar{n}_p$ by more than 2σ in Figure 3. This occurs for both the northern and southern clusters at $z \sim 0.10$.

5. The Cluster Spatial Correlation Function

We use the following estimator derived in Hamilton (1993) for the determination of the correlation function:

$$\xi(r) = \frac{DD(r) \times RR(r)}{DR(r)^2} - 1, \tag{5}$$

where DD, RR, and DR are the data-data, random-random and data-random paircounts respectively with separations between $r - \frac{\Delta r}{2}$ and $r + \frac{\Delta r}{2}$. We refer the reader to Hamilton (1993) and Landy & Szalay (1993) for an analytical analysis of the estimator. Compared to previous estimators (see Bahcall & Soneira (1983) and PHG), this one is proposed to be less affected by uncertainties in the mean number density where separations are large and ξ is small. Recently, Ratcliffe *et al.* (1998) used N-body simulations to show that the Equation (5) provided the most accurate results when compared to other estimators.

The random paircounts (DR, RR) are evaluated by averaging over 400 catalogs generated with the same number of pseudo-clusters as the sample under consideration. The angular coordinates in these catalogs are randomly assigned with the same boundary conditions as the survey and with a galactic latitude selection function,

$$P(b) = 10^{\alpha(1-csc|b|)}, \tag{6}$$

with $\alpha = 0.32$ imposed to account for residual galactic obscuration after the latitude cut at $|b| = 30^\circ$ (PHG, Peacock & West 1992). The redshifts assigned to the random catalog points are selected from the observed data after being smoothed with a Gaussian of width 3000 km s^{-1}. This technique corrects for radial density gradients on small scales in the observed distribution. For the whole-sky sample, the random points with $\delta \geq -17^\circ$ are assigned redshifts from the Abell clusters, while the points with $\delta \leq -17^\circ$ are assigned redshifts from the ACO catalog. We have chosen to limit the cluster redshifts in the Whole-sky sample to $z = 0.10$ where the average densities begin to drop off dramatically. However, by using the observed redshifts for our random catalogs, we are effectively modeling any selection effects in z, making the chosen limit of $z = 0.10$ somewhat arbitrary.

The spatial correlation function for luminous mass concentrations has been shown by various authors to have the following power-law form:

$$\xi(r) = (\frac{r}{r_0})^\gamma. \tag{7}$$

For galaxy-galaxy spatial correlations, $r_0 \approx 5h^{-1}$Mpc and $\gamma = -1.8$ (see Willmer *et al.* (1998) for a review of galaxy-galaxy correlation function results). However, cluster-cluster correlation results have been more uncertain (see Table 1.) Bahcall & Soneira (1983) originally found $r_0 \approx 24h^{-1}$Mpc and $\gamma = -1.8$. However, the small size of this sample, 104

$R \geq 1$ clusters, and its use of many single-redshift clusters leave considerable uncertainty in those results. PHG later found similar results for γ and r_0 with a slightly larger sample of 156 $R \geq 1$ clusters. We reexamined this sample, with a galactic latitude cut of $|b| \geq 30^\circ$ to minimize any effects in the Abell catalog due to obscuration by the Galaxy. The final sample of 126 clusters is very similar to the Bahcall & Soneira (1983) sample and we expect the same results (and large uncertainties). Our tests produced results nearly identical to those reported by PHG (Table 1), although we would not have been surprised to see small differences as a result of a few different redshifts for clusters that had previously had only one measured redshift (before the MX survey).

Soon after the PHG results, Peacock and West (1992) compiled a volume-limited (to $z = 0.08$) sample of 195 $R \geq 1$ Abell and ACO clusters and found a reduced $r_0 = 21h^{-1}$Mpc and increased $\gamma = -2.0$. It should be noted that Peacock & West did not use a magnitude limit for their sample and the data was not complete beyond $m_{10} \geq 16.5$, although many clusters with $m_{10} > 16.5$ were used. It is highly probable that the $m_{10} \geq 16.5$ subset of clusters used in the Peacock & West sample was not a fair sampling. Many dimmer clusters were observed for a specific reason (such as being a supercluster member, particularly rich, containing substructure, etc). The use of such incomplete datasets raises the risk of detecting spurious structure due to sampling effects. There have been other determinations of r_0 and γ for Abell clusters via cD clusters and X-ray clusters selected from within the Abell catalog with results $16 \leq r_0 \leq 22(h^{-1}\text{Mpc})$ and $-1.9 \geq \gamma \geq -1.7$ (West & van den Bergh 1991; Nichol *et al.* 1994).

With the recent evidence for redshift-versus-sky-position inhomogeneities in samples of Abell clusters (presumably from the visual selection of clusters) (Sutherland 1988; Efstathiou *et al.* 1992), several groups have conducted redshift surveys of catalogs of clusters produced through machine-scanning of sky-survey plates, *e.g.* the APM galaxy survey (Maddox *et al.* 1990a,b) and the EDSGC cluster catalog (Lumsden *et al.* 1992). The correlation length for clusters selected from the APM catalog show $13 \leq r_0$ (h^{-1}Mpc) ≤ 15 and $\gamma \approx -2$ (Efstathiou *et al.* 1992; Dalton *et al.* 1994). These determinations are based on samples with large numbers (up to 364) of more common, less rich clusters within an area on the sky of 1.3 steradians. The correlation length for the EDSGC clusters was reported to be $r_0 = 16.2 \pm 2.3$ with $\gamma = -2.0 \pm 0.2$ (Nichol *et al.* 1992). A list of results for the slope and correlation length for the various determinations of ξ are listed in Table 1.

The large difference between the Abell cluster correlation length and that of the plate scanned cluster catalogs has been the subject of much debate. Unfortunately, until this work, the samples of Abell clusters analyzed were either small with many clusters having only one measured galaxy redshift (Bahcall & Soneira 1983), incomplete in magnitude

(Peacock & West 1992), or contained $R = 0$ clusters (PHG). This work eliminates all of these problems with a large magnitude-complete sample of $R \geq 1$ Abell/ACO clusters. We present our two-point correlation function results in the next section.

5.1. Results for the MX Survey Sample

Figure 4 shows the results for the spatial correlation function for the four different samples defined in Section 3. The three lines on the graphs indicate two enveloping limits that span the results in Table 1 ($r_0 = 25$, $\gamma = -1.8$ and $r_0 = 15$ and $\gamma = -2.0$) and the best power-law fit for $\xi(r)$ from our data points (from $r = 4h^{-1}$Mpc to $35h^{-1}$Mpc). The error bars plotted in Figure 4 are determined from

$$\delta\xi = \frac{(1+\xi)}{\sqrt{DD}}. \tag{8}$$

However, we note that Croft & Efstathiou (1994) have shown that this underestimates the true error by a factor of $1.3 \rightarrow 1.7$. We have excluded the bins of smaller separations ($r \leq 4.5h^{-1}$Mpc) from the fit for the following reasons: (1) the number of data-data pairs at small separations becomes unreasonably small; (2) we get nearer to the actual diameter of a rich Abell cluster where projection effects compromise differentiation from a foreground and background cluster; and (3) the $\sim$500 km s^{-1} cluster peculiar velocities mentioned in Section 2 will mask structure. Notice that the amplitudes in Figure 4a-d are similar to that of previous, smaller samples used by Bahcall & Soneria (1983) and PHG, yet only the cD clusters show strong correlations beyond $r \sim 25h^{-1}$Mpc. These results, listed in Table 2, provide strong support for previous claims of a large two-point correlation function amplitude. Yet at the same time, we find only minimal correlations beyond $r \sim 25h^{-1}$Mpc for the northern magnitude-limited sample and both whole-sky samples. We point out that using an older estimator (*e.g.* $\frac{DD}{RR} - 1$) shows slightly larger correlations out to $\sim 50h^{-1}$Mpc before going negative.

The slopes and correlation lengths are similar for all the datasets examined, including the cD cluster sample (which is significantly different from the other samples since it contains $R = 0$ clusters). All four samples examined have $19.4 \leq r_0 \leq 23.4(h^{-1}$Mpc) and $-1.92 \leq \gamma \leq -1.83$. On large scales, we find that $\xi(r)$ becomes negative at $\sim 50h^{-1}$Mpc, although the error on ξ in this region is comparable to ξ itself. The increased number of redshifts, in addition to the increased accuracy of those redshifts due to multiple-galaxy observations, has produced a much improved fit (with much smaller errors) to the rich cluster correlation function. These results, based on the largest and most complete sample of rich clusters assembled to date, show that the correlation length for $R \geq 1$ Abell clusters

is significantly larger ($\sim 3\sigma$) than results for the APM survey.

5.2. The Effects of Superclusters on r_0

The effect of the Corona Borealis supercluster (Cor Bor) on the amplitude of the correlation was illustrated in Postman *et al* (1988) and again in PHG. Using the Bahcall & Soneira (1983) $D \leq 4$, $R \geq 1$ sample of clusters, Postman *et al.* (1988) concluded that Cor Bor is responsible for $\sim 30\%$ of the amplitude of $\xi(r)$. They later reexamined this effect using a larger sample of $R \geq 1$ clusters and found that Cor Bor contributed slightly less, $\sim 20\%$ (Postman, Huchra and Geller, 1992). Using the whole-sky magnitude-limited sample of $R \geq 1$ clusters, we find that r_0 decreases by $\sim 8\%$ after excluding Cor Bor (A2061, A2065, A2067, A2079, A2089, A2092) (see Table 2). We find a slightly larger reduction in r_0 after excluding the newly discovered dense and compact supercluster in Microscopium. This supercluster consists of A3677, A3682, A3691, A3693, A3695 and A3705 and was first reported by Zucca *et al.* (1993) and many redshifts were observed by ENACS (Kagert *et al.* 1996). The exclusion of the Microscopium Supercluster (MSC) reduces r_0 by $\sim 13\%$. Together, the removal of Cor Bor and Microscopium reduces r_0 by 20% (from $23.4h^{-1}$Mpc to $18.4h^{-1}$Mpc) and steepens the slope from $\gamma = -1.83$ to $\gamma = -2.13$. It is important to note that this lower value of r_0 is within 1σ of the value obtained for the APM cluster results (Efstathiou *et al.* 1992) and that both Cor Bor and the MSC lie outside of the right ascension and declination limits of the APM Survey.

While the effects on the correlation function from individual superclusters seem to diminish as we increase the sample size, we are finding more of these dense and compact superclusters as we extend the survey to greater depths. In fact, Batuski *et al.* (1999) have recently discovered a collection of six Abell/ACO clusters at $z = 0.11$ with a spatial number overdensity similar to that of the Corona Borealis supercluster. Thus, including the Shapley Concentration, we now have four such dense, compact superclusters in the local Universe. The existence of these superclusters has a clear impact on the correlation function amplitude and slope. (We note that most of the Shapley Concentration does not appear in these analyses due to the imposed galactic latitude limit of $|b| \geq 30°$.)

6. Anisotropy in the Abell catalog

The amplitude of the two-point spatial correlation function for clusters has been a controversial subject since the seminal work by Bahcall & Soneira (1983). Soon after their

report that $r_0 \sim 25h^{-1}$Mpc for rich clusters, numerical simulations based on the standard model ($\Omega = 1$, CDM) were conducted that failed to reproduce this high amplitude after normalization to the galaxy distribution or the cosmic microwave background (Bardeen, Bond, Efstathiou 1987; White *et al.* 1987). In addition, analytical work by Kaiser (1984) showed that if clusters form at the high density peaks of Gaussian random fields, then we expect the cluster correlation function to approach the matter correlation function at large separations, and the matter two-point spatial correlation function is predicted to become negative at $\sim 20(\Omega h^2)^{-1}$ in a CDM Universe (Davis *et al.* 1985). Yet the observed two-point correlation function for rich clusters remains positive out to $\sim 50h^{-1}$Mpc.

In response to the simulation and analytical results, Sutherland (1988) proposed that the high amplitude of r_0 for the Abell catalog was the result of the spurious enhancement of the number of cluster pairs at small separations. 'Corrective' techniques were created to account for these supposed anisotropies which reduced the value of r_0. These techniques (see Sutherland (1988) or Efsathiou *et al.* (1992)) typically subtracted out individual clusters or cluster pairs that were too close together on the plane of the sky. Other explanations for the anisotropy (excess pairs with small angular separations) detected in the Abell catalog have been suggested. Bahcall, Soneira & Burgett (1986) have proposed that the anisotropy could be caused by the finger-of-God effect or possibly supercluster elongation. Jing, Plionis, & Valdarnini (1992) found that the elongation of cluster pairs in the redshift direction occurred nearly as often (15% to 30% of the cases) in model universes (with pseudo-clusters placed near the peaks of a Gaussian density field) as in the Abell catalog. Peacock & West (1992) found that most of the anisotropies were in the statistically incomplete subset of $R = 0$ clusters. We will show that the $R \geq 1$ subset of Abell clusters contains only a residual amount of anisotropies which can be accounted for by specific superclusters, elongated roughly along the line-of-sight.

To search for this anisotropy, we examined $\xi(r)$ after separating r into its line of sight component and the component perpendicular to the line of sight (Sutherland 1988):

$$r^2 = \sigma^2 + \pi^2 \tag{9}$$

where

$$\pi = |z_1 - z_2| \tag{10}$$

Figure 5 shows contour plots of $\xi(\sigma, \pi)$ over the range $0 - 100h^{-1}$Mpc for both σ and π, in 10 h^{-1}Mpc bins. The heavy contour line is $\xi(\sigma, \pi) = 1$, indicating relatively strong correlations. These types of plots have been used by numerous authors as an indicator of line-of-sight anisotropy within cluster catalogs (Peacock & West 1992; Efstathiou *et al.* 1992; Nichol *et al.* 1992; Dalton *et al.* 1994). However, a review of the literature shows

some confusion in the interpretation of these plots. Therefore, we will first examine the PHG dataset and discuss why (and where) it has been shown to be anisotropic.

Figure 5a recreates $\xi(\sigma, \pi)$ for the PHG statistical sample. This sample was used by Efstathiou *et al.* (1992) to contrast with the APM sample. The reader will notice a region of strong correlation with $\sigma \leq 20h^{-1}$Mpc and $50 \leq \pi \leq 80h^{-1}$Mpc. The most probable explanation for these correlations is the preferential selection of clusters nearby on the plane of the sky with relatively large separations in redshift. This indicates that some of the clusters, within the pairs that are causing these high correlations, should have been classified with a lower richness (and possibly not even $R \geq 0$ clusters at all). We must also recognize the level of incompleteness in the $R = 0$ subset of Abell clusters as a contributor to these anisotropies, although it is difficult to say exactly what effect this would have. Strong correlations in this region of σ and π indicate observational bias within the sample examined. Peacock & West (1992) noticed this anisotropy in a volume-limited sample of $R = 0$ Abell clusters and recommended that $R = 0$ clusters not be used in statistical analyses. The reader will also notice the area of strong correlations with $\sigma \leq 20h^{-1}$Mpc and $\pi \leq 40h^{-1}$Mpc. This 2:1 elongation of $\xi(\sigma, \pi)$ in the strong clustering region can be explained by a number of effects: high cluster peculiar velocities ($\sim$ 1500 km s^{-1}), a large number of pairs with small angular separations and moderate redshift separations, or real geometric elongation of superclusters with multiple cluster members distributed along the line-of-sight. While line-of-sight anisotropy is also an explanation, it is not the only possibility.

Contour plots, such as Figure 5, have been widely used to compare machine plate-scanned surveys with the Abell catalog (Efstathiou *et al.* 1992; Nichol *et al.* 1992; Dalton *et al.* 1994). The conclusion from these analyses is that plate-scanned catalogs (such as the APM and EDSGC catalogs) do not suffer from the anisotropy as seen in the PHG Abell cluster sample (Figure 5a). Results from APM cluster analyses by Efstathiou *et al* and Dalton *et al.* show no correlations for small σ and large π ($50 \leq \pi \leq 80h^{-1}$Mpc), yet there is a similar 2:1 elongation of $\xi(\sigma, \pi)$ in the strong clustering region. In contrast to the APM catalog, the Nichol *et al.* analysis of the EDSGC cluster catalog reports no elongation in the strong clustering region. However, Figure 2a in Nichol *et al.* clearly shows strong correlation where σ is small and π is large (50 - 80 h^{-1}Mpc) (This is a strong indication of selection bias and is not discussed by Nichol *et al.*).

Figures 5b-d show isocontours of $\xi(\sigma, \pi)$ for the Northern magnitude-limited, whole-sky magnitude-limited and whole-sky statistical samples. Notice that the strong correlations with $\sigma \leq 20h^{-1}$Mpc and $50 \leq \pi \leq 80h^{-1}$Mpc are no longer evident in these $R = ge1$ cluster samples. We remind the reader that only the $R \geq 1$ clusters were defined as a

statistically complete sample by Abell (1958). Unfortunately, until now, there simply were not enough $R \geq 1$ cluster redshifts to perform such an analysis for a magnitude-limited sample. While the strong indication of anisotropy is no longer evident in Figures 5b-d, there is a residual anisotropy evident in the 2:1 elongation of $\xi(\sigma, \pi)$ (where $\sigma \leq 20h^{-1}$Mpc and $0 \leq \pi \leq 40h^{-1}$Mpc).

For the sake of clarity, we will perform all further analyses solely on the whole-sky magnitude-limited sample. This choice is based on the large number of clusters in this sample and the similarities in the correlation function results between the whole-sky magnitude-limited and the whole-sky statistical samples (see Figures 4b,c and 5c,d).

6.1. The Effects of Elongated Superclusters

We determined which cluster pairs were causing the excess in $\xi(\sigma, \pi)$ in the region where $\sigma \leq 10h^{-1}$Mpc and $20 \leq \pi \leq 40h^{-1}$Mpc. There are 19 pairs within these ranges of σ and π and we discovered that eight (8) of these were associated with either the Corona Borealis supercluster or the Ursa Majoris supercluster. Random catalogs produced only ~ 8 pseudo-cluster pairs within these ranges of σ and π. Using methods similar to that of Jaaniste *et al.* (1998), we fit ellipsoids to the clusters within the two superclusters to determine their shapes and orientations. Ursa Majoris is comprised of clusters A1291, A1318, A1377, A1383, and A1436. Its ellipsoidal fit produces the axis ratio 1.0:0.2:0.1, which is highly filamentary. The angle between the semi-major axis and the line-of-sight is 14°. We also fit the six major clusters in Cor Bor (A2061, A2065, A2067, A2079, A2089, and A2092) producing the axis ratio of 1.0:0.4:0.25 with the angle between the semi-major axis and the line-of-sight at 22°. We note these results are slightly different from those of Jaaniste *et al.* due to the fact that we are using only $R \geq 1$ clusters. While it is obvious that the (excess) pairs with $\sigma \leq 10h^{-1}$Mpc and $20 \leq \pi \leq 40h^{-1}$Mpc are mostly members of superclusters that are elongated roughly along the line of sight, it is not so obvious that these pairs are the cause of the elongation of $\xi(\sigma, \pi)$ in this region.

While we could remove these superclusters from the catalog and re-examine the contour plots of $\xi(\sigma, \pi)$, we saw in the previous section that this could affect the amplitude and slope of the standard two-point correlation function, $\xi(r)$. By removing certain clusters from the catalog we are altering the inherent structure of the catalog (unless, of course, the clusters removed are spurious). Instead, we have chosen to rotate these superclusters until their semi-major axes are perpendicular to the line-of-sight. We then recalculated the standard two-point correlation function and found no difference in the amplitude or slope (see Figure 6 and Table 2). Figure 7 shows the isocontours of $\xi(\sigma, \pi)$ for the new whole-sky

magnitude-limited sample with the Ursa Majoris and Corona Borealis superclusters rotated so that their semi-major axes are nearly perpendicular to the line-of-sight. The region of strong clustering shows no elongation whatsoever, and there are only very weak correlations beyond $25h^{-1}$Mpc.

At this point, we need to qualify the reality of these two superclusters, Ursa Majoris and Corona Borealis. All of the clusters within these superclusters have multiple observed galaxy redshifts, although Corona Borealis has been studied in greater detail (Schuch, 1981, 1983; Postman *et al.* 1986, 1988; Small *et al.* 1997a,b, 1998). PHG, whose dataset included both the Ursa Majoris and the Corona Borealis superclusters, looked for contamination within their sample by recreating the spatial distribution of $R \geq 0$ clusters using realistic cluster profiles. They found only five $R \geq 1$ clusters that show contamination, one of which was A2061 within Corona Borealis. When A2061 is excluded from our samples, we find no difference in any of our results. According to PHG, none of the clusters in Ursa Majoris show contamination. While the MX Survey has added ~ 70 new northern clusters in the magnitude extension to $m_{10} = 16.8$, none of these clusters are near enough to Ursa Majoris or Corona Borealis to cause new possible contaminations related to those superclusters.

Since projection contamination has been suggested as a reason for dismissing the Abell catalog for large-scale structure studies, it is worthwhile examining even the most unlikely case where the Ursa Majoris supercluster contains mostly $R = 0$ clusters (or poor groups) suffering from extreme projection (thus inflating apparent richnesses). In this analysis, we find no change in the correlation length or slope (see Table 2) after excluding four of the five Ursa Majoris cluster members from the catalog. We can take this analysis one step further and exclude *any* Abell/ACO clusters that show projection problems. In this case, we looked at the galaxy velocity distributions for clusters published in Zabludoff *et al.* (1993), Mazure *et al.* (1996), and Slinglend *et al.* (1998). We reduced the richness classification by one level whenever the total number of galaxies within any cluster was less than 60% of the total number of galaxies observed in the cluster field. (Note: some of the ACO clusters had already been excluded by the $N_{gal} \geq 54$ cut-off.). In the end, we excluded 19 clusters from the original 289 in the whole-sky magnitude-limited sample (an additional five clusters were reduced from $R = 2$ to $R = 1$). After re-examining the two-point correlation function, we find almost no change in the correlation length or slope (see Table 2).

The reader may also be concerned with the fact that we have detected two elongated superclusters along the line-of-sight within a catalog that contains a small number of superclusters. To examine the probability of such an event, we performed percolation analyses on the whole-sky magnitude-limited sample at two percolation lengths, $b = 20h^{-1}$Mpc and $b = 30h^{-1}$Mpc, corresponding to spatial density enhancements $(n/\bar{n})$

of ~ 20 and ~ 5. At $b = 20h^{-1}$Mpc we find seven superclusters with five or more cluster members and four of these superclusters show elongation similar to or greater than that of Corona Borealis. To see how often we would expect one of these elongated superclusters to lie within 25° of the line-of-sight (recall, the semi-major axis of Corona Borealis is 22° off the line-of-sight) we perform a geometrical calculation among randomly oriented structures. The probability of finding a single elongated supercluster along the line-of-sight is equal to the solid angle of a circle with diameter 25° divided by 2π steradians or ~ 0.10. The probability of finding one of the four elongated superclusters along the line-of-sight is ~ 0.30. There is a 10% chance of finding two of these four superclusters to lie within 25° of the line-of-sight. At $b = 30h^{-1}$Mpc we find eight superclusters with five or more cluster members and five of these superclusters show elongation similar to or greater than that of Corona Borealis. In this case, there is a 15% chance of finding two of the five elongated superclusters to lie within 25° of the line-of-sight. These results indicate that if four (or five) elongated superclusters were randomly oriented in space, a central observer would have reasonable chance, 10% - 15%, of finding two superclusters within 25° of the line-of-sight. Finding two such superclusters in the Abell/ACO catalogs is modestly probable. We refer the reader to Batuski *et al.* (1999) for a more detailed examination of filamentation in the Abell/ACO catalogs.

From this analysis, we can conclude that two evidently real structures, elongated along the line-of-sight, are the cause of the previously detected anisotropy within the Abell/ACO catalogs. The 2:1 elongation of $\xi(\sigma, \pi)$ seen in Figures 5b-d would not appear in these contour plots, had the two superclusters been oriented perpendicular to the line-of-sight. Thus, the anisotropy present in Figures 5b-d is the result of superclustering along the line of sight, not an indicator of observational bias or high peculiar velocities. In addition, the fact that we can remove this anisotropy from the catalog (via supercluster rotation) *without* changing r_0 calls the previously mentioned 'corrective' techniques into question.

Figures 5 and 7 indicate the level of anisotropy in a visual, somewhat qualitative way. Attempts have been made to quantify this anisotropy by convolving the derived form of the correlation function with a Gaussian of chosen width (Peacock & West 1992; Estathiou *et al.* 1992; Dalton *et al.* 1994):

$$\xi(\sigma, \pi) = \frac{r_0^{-\gamma}}{\sqrt{2\pi}\sigma_v} \int_{-\infty}^{\infty} [\sigma^2 + (\pi - x)^2]^{\gamma/2} e^{\frac{-x^2}{2\sigma_v{}^2}} dx. \tag{11}$$

This attempts to match the observed $\xi(\sigma, \pi)$ with the $\xi(r)$ obtained from the best power law fit. We must also note that an assumed Gaussian distribution for ξ is most likely inappropriate because of ξ's power-law form. This is not an attempt to determine cluster peculiar velocities. We are merely providing these results for comparison to other such

analyses.

For this analysis, we can look only at a region constrained by $0 \leq \sigma \leq 15$ (h^{-1}Mpc) where the number of paircounts is appreciable. Figure 8a shows $\xi(\sigma, \pi)$ plotted against π for cluster pairs with projected separations in the range $0 \leq \sigma \leq 15(h^{-1}\text{Mpc})$ and total separations $r \leq 100h^{-1}$Mpc. The solid histogram is the PHG statistical sample while the dash-dot histogram is the whole-sky magnitude-limited sample. The smooth lines are the respective histograms convolved with a Gaussian as in Equation (11) with $\sigma_v = 700$ km s^{-1} and the appropriate slope and correlation length. As an indicator of anisotropy within a cluster sample, we measure the mean value of $\xi(\sigma, \pi)$ for $\sigma \leq 15h^{-1}$Mpc and $\pi \geq 20h^{-1}$Mpc where we expect $\xi(\sigma, \pi)$ to be small. The mean values of the correlation function beyond $\pi = 20h^{-1}$Mpc are $\bar{\xi}(\sigma, \pi) = 0.53 \pm 0.56$ for the PHG sample and $\bar{\xi}(\sigma, \pi) = 0.32 \pm 0.60$ for the whole-sky sample. Notice the large reduction in $\xi(\sigma, \pi)$ beyond $40h^{-1}$Mpc between the PHG sample and the whole-sky sample. Figure 8b compares the whole-sky sample before and after the Ursa Majoris and Cor Bor supercluster rotations. Again, the curves are the respective histogram convolved with a Gaussian. Notice the drop in correlation in the range $20 \leq \pi \leq 50h^{-1}$Mpc. This is consistent with the drop in correlations noticeable in Figures 5c and 7. The mean value of the correlation function beyond 20 h^{-1}Mpc for the rotated case is $\bar{\xi}(\sigma, \pi) = 0.16 \pm 0.49$. While the PHG case shows some strong correlations out to $70h^{-1}$Mpc, the new $R \geq 1$ whole-sky magnitude-limited sample has essentially no detectable correlations beyond $40h^{-1}$ Mpc. After rotating the Ursa Majoris and Corona Borealis superclusters so that they are not elongated along the line of sight, we find no detectable correlations beyond $20h^{-1}$ Mpc. This is comparable to the claims made by Efstathiou *et al.* (1992) that the APM cluster catalog shows no line-of-sight correlations beyond $25h^{-1}$Mpc. An analysis of Figure 3 in Efstathiou *et al.* (1992) shows $\bar{\xi}_{APM}(\sigma, \pi) \sim 0.10$ beyond $20h^{-1}$Mpc, which is very similar to what we find in the Abell/ACO catalogs after rotating the two superclusters.

7. Conclusion

The results presented in this work provide strong evidence for the *lack* of observational selection bias and projection effects in the $R \geq 1$ sample of Abell clusters. While some earlier studies indicated that anisotropies and spurious cluster selection greatly affected correlation analyses, those results were based on smaller and/or incomplete samples, samples with a large number of single-redshift cluster distances, and samples containing $R = 0$ clusters. The MX Survey has provided a large, complete dataset of multiple-redshift $R \geq 1$ Abell cluster distances for analyses of large-scale structure in the local universe.

We have calculated the mean space density of $R \geq 1$ clusters to be $\bar{n}_p = 6.6(\pm 0.6) \times 10^{-6} h^3 \mathrm{Mpc}^{-3}$ for the northern Abell clusters and $\bar{n}_p = 7.6(\pm 0.9) \times 10^{-6}$ $h^3 \mathrm{Mpc}^{-3}$ for the southern ACO clusters. This result supports previous claims that the ACO catalog includes slightly poorer $R \geq 1$ clusters than the northern Abell catalog. Power-law fits of the two-point spatial correlation function of the MX samples are presented in Table 2 and in Figure 4. We find $19.4 \leq r_0 \leq 23.4 h^{-1}\mathrm{Mpc}$, $-1.92 \leq \gamma \leq -1.83$ for the different subsets of $R \geq 1$ clusters examined.

We have used the largest rich cluster data set available to date to look for line-of-sight anisotropies within the Abell/ACO catalogs. An examination of the correlation function separated into its line-of-sight (π) and perpendicular-to-line-of-sight (σ) components show that the strong anisotropy present in the PHG sample (where $\xi(\sigma, \pi) > 1$ with $\sigma \leq 20 h^{-1}\mathrm{Mpc}$ and $50 \leq \pi \leq 80 h^{-1}\mathrm{Mpc}$ in Figure 5a) is not present in our samples (Figures 5b-d). The remaining anisotropies in our samples, indicated by the 2:1 elongation of $\xi(\sigma, \pi)$ (where $\sigma \leq 20 h^{-1}\mathrm{Mpc}$ and $\pi \leq 40 h^{-1}\mathrm{Mpc}$), can be explained by the orientation of two elongated superclusters, Ursa Majoris and Corona Borealis. After rotating these well-established superclusters so that their semi-major axes are perpendicular to the line-of-sight, we find no indication of anisotropy in the contour plots of $\xi(\sigma, \pi)$ (see Figure 7). Therefore, the 2:1 elongation of $\xi(\sigma, \pi)$ can be considered a true characteristic of the sample examined, not an indicator of line-of-sight selection biases.

We performed percolation analyses on the whole-sky magnitude-limited sample and find 4-5 elongated superclusters with axes ratio of 2.5:1:1 or greater (depending on the choice of percolation length). If these elongated superclusters were distributed in space with random orientations, the probability of finding two within 25° of the line-of-sight is 10% - 15%, which is not unduly unlikely. Thus, it is not surprising to find anisotropies (as detected by contour plots of the correlation function) as the result of superclustering along the line-of-sight.

The correlation length and slope of the two-point spatial correlation function, $\xi(r)$, are very robust for the whole-sky magnitude-limited sample. After rotating Ursa Majoris and Corona Borealis so that they are perpendicular to the line-of-sight, both r_0 and γ remain unchanged. Since these rotations remove any evidence of line-of-sight anisotropies within the catalog, we conclude that r_0 is not inflated (compared to the APM clusters) by these anisotropies. We also find no change in r_0 and γ after excluding 19 clusters (from various sources) that may have heavy foreground/background contamination. This work conflicts with earlier conclusions by Sutherland (1988) (whose results were then expanded upon in Efstathiou *et al.* (1992) and Nichol *et al.* (1992)), that the Abell catalog suffers from a large amount of spurious cluster selection which, in turn, inflates r_0. While there are certainly

individual clusters that show heavy background/foreground contamination, they make up only 10% of the total in our magnitude-complete samples and their exclusion has no effect on the amplitude or slope of the correlation function. If, however, we remove actual structures from the dataset, such as the Corona Borealis and Microscopium superclusters, r_0 decreases (by up to 20%) and γ steepens (from ~ 1.8 to $2.1h^{-1}$Mpc). The high value of r_0 for $R \geq 1$ Abell clusters continues to rule out the standard CDM models and future simulations must be able to reproduce large-scale clustering out to scales of $\sim 50h^{-1}$Mpc.

We wish to thank Adrian Melott for helpful discussions on the manuscript.

KAS, DJB and CM were supported in this work by National Science Foundation Grant AST-9224350.

CM was funded in part by the National Aeronautics and Space Administration and the Maine Science and Technology Foundation

This research has made use of the NASA/IPAC Extragalactic Database (NED), which is operated by the Jet Propulsion Laboratory, California Institute of Technology, under contract with the National Aeronautics and Space Administration.

REFERENCES

Abadi, M., Lambas, D., and Muriel, H. 1998, ApJ, 507, 526

Abell, G. O. 1958, ApJS, 3, 211

Abell, G. O., Corwin, H. G., Olowin, R. P. 1989, ApJS, 70, 1 (ACO)

Bahcall, N.A. & Cen, R. 1994, ApJ, 426, L15

Bahcall, N.A., Oh, S.P. 1996, ApJ, 462, L49

Bahcall, N., Soniera, R. 1983, ApJ, 270, 20

Bahcall, N., Soneira, R., and Burgett, W. 1986, ApJ, 311, 15

Bahcall, N.A. & West, M.J. 1992, ApJ, 392, 419

Bardeen, J.M., Steinhardt, P.J., & Turner, M.S. 1983, Phys. Rev. D, 28, 679

Bardeen, J.P., Bond, J.R., & Efstathiou, G. 1987, ApJ, 321, 28

Batuski, D. J., Burns, J. O. 1985, ApJ, 299, 5

Batuski, D.J, Bahcall, N.A, Burns, J.O., & Olowin, R. 1989, ApJ, 341, 599

Batuski, D.J., Miller, C.J., Slinglend, K.A., Balkowski, C., Maurogordato, S., Cayatte, V., Felenbok, P., & Olowin, R. 1999, Under revision for ApJ

Croft, R.A.C., & Efstathiou, G. 1994, MNRAS, 267, 390

Dalton, G.B., Croft, R.A.C., Efstathiou, G., Sutherland, W.J., Maddox, S.J., and Davis, M. 1994, MNRAS, 271, 47

Davis, M., Efstathiou, G., Frenk, C.S., & White, S.D.M. 1985, ApJ, 292, 371

Ebeling, H., Edge, A.C., Fabian, A.C., Allen, S.W., Crawford, C.S., Boehringer, H. 1997, ApJ, 479, L101

Efstathious, G., Dalton, G.B., Maddox, S.J., & Sutherland, W. 1992, MNRAS, 257, 125

Geller, M., & Huchra, J.P. 1989, Science, 246, 897

Guth, A.H., & Pi, S-Y. 1982, Phys. Rev. Lett., 49, 1110

Hamilton, A.J.S. 1993, ApJ, 417, 19

Huchra, J.P., Henry, J.P., Postman, M., & Geller, M.J. 1990, ApJ, 365, 66

Jaaniste, J., Tago, E., Einasto, M., Einasto, J., Andernach, H., Mueller, V. 1998, A & A, 336, 35

Jing, Y.P., Plionis, M., Valdarnini, R. 1992, ApJ, 389, 499

Kaiser, N. 1984, ApJ, 284, 9

Katgert,P., Mazure, A., Perea, J., den Hartog, R., Moles, M., Le Fevre, O., Dubath, P., Focardi, P., Rhee, G., Jones, B., Escalera, E., Biviano, A., Gerbal, D., Giuricin, G. 1996, A & A, 310, 8

Kolb, E.W. & Turner, M.S. 1990, The Early Universe, Addison-Wesley Publishing Company

Landy, S.D. & Szalay, A.S. 1993, ApJ, 412, 64

Linde, A. 1982, Phys. Lett. B, 108, 389

Ling, E.N., Frenk, C.S., Barrow, J.D. 1986, MNRAS, 223, 21

Lucey, J.R. 1983, MNRAS, 203, 33

Lumsden, S.L., Nichol, R.C., Collins, C.A., & Guzzo, L. 1992, MNRAS, 258, 1

Maddox, S.J., Sutherland, W.J., Efstathiou, G., Loveday, J. 1990a, MNRAS, 243, 692

Maddox, S.J., Efstathiou, G., Sutherland, W.J. 1990b, MNRAS, 246, 443

Mazure, A. *et al.* 1996, MNRAS, 310, 31

Miller, C.J., Slinglend, K.A., Batuski, D.J., & Hill J.M. 1999, in preparation

Narlikar, J.V. 1983, Introduction to Cosmology, Cambridge University Press

Peacock, J.A. & West, M.J. 1992, MNRAS, 259, 494

Nichol, R.C., Collins, C.A., Guzzo, L., & Lumsden, S.L. 1992, MNRAS, 255, 21

Nichol, R.C., Briel, U.G., & Henry, J.P. 1994, MNRAS, 267, 771

Postman, M., Huchra, J. P., & Geller, M. J. 1986, AJ, 92, 1238

Postman, M., Geller, M. J., & Huchra, J.P. 1988, AJ, 95, 267

Postman, M., Huchra, J. P., & Geller, M. J. 1992, ApJ, 384, 404

Quintana, H. & Ramirez, A. 1995, ApJS, 96, 343

Ratcliffe, A., Shanks, T., Parker, Q. & Fong, R. 1998, MNRAS, 296, 173.

Sandage, A. 1975, Stars and Stellar Systems: Galaxies and the Universe, University of Chicago Press

Schombert, J.M. & West, M.J. 1990, ApJ, 363, 331

Schuch, N. 1981, MNRAS, 196, 695S

Schuch, N. 1983, MNRAS, 204, 1245S

Shectman, S.A., et al. 1996, ApJ, 470, 172

Slinglend, K.A., Batuski, D.J, Miller, C.M., Haase. S., Michaud, K., & Hill, J.M. 1998, ApJS, 115, 1

Small. T., Sargent, W., & Hamilton, D. 1997, ApJS, 111, 1

Small. T., Sargent, W., & Hamilton, D. 1997, ApJ, 487, 512

Small. T., Ma, C., Sargent, W., & Hamilton, D. 1997, ApJ, 492, 45

Struble, M.F & Ftaclas, C. AJ, 108, 1

Struble, M.F. & Rood, H.J. 1987, ApJS, 63, 543

Struble, M.F. & Rood, H.J. 1991, ApJ, 374, 395

Sutherland, W. 1988, MNRAS, 234, 159

Szalay, A. & Schramm, D. 1985, Nature, 314, 718

Turok, N. 1989, Phys. Rev. Lett., 63, 2625

Vilenkin, A. 1981, Phys. Rev. Lett., 46, 1169

West, M.J., and van den Bergh, S. ApJ, 373, 1

White, S.D.M., Davis, M., Efstathiou, G., & Frenk, C.S. 1987, Nature, 330, 451

Willmer, C., Da Costa, L.N., & Pellegrini, P.S. 1998, AJ, 115, 869

Zabludoff, A., Geller, M., Huchra, J.P., & Vogeley, M. 1993, AJ, 106, 1273

Zeldovich, Ya.B., 1980, MNRAS, 192, 663

Zucca, E., Zamorani, G., Scaramella, R., & Vettolani, G. 1993, ApJ, 407, 470

This preprint was prepared with the AAS LaTeX macros v4.0.

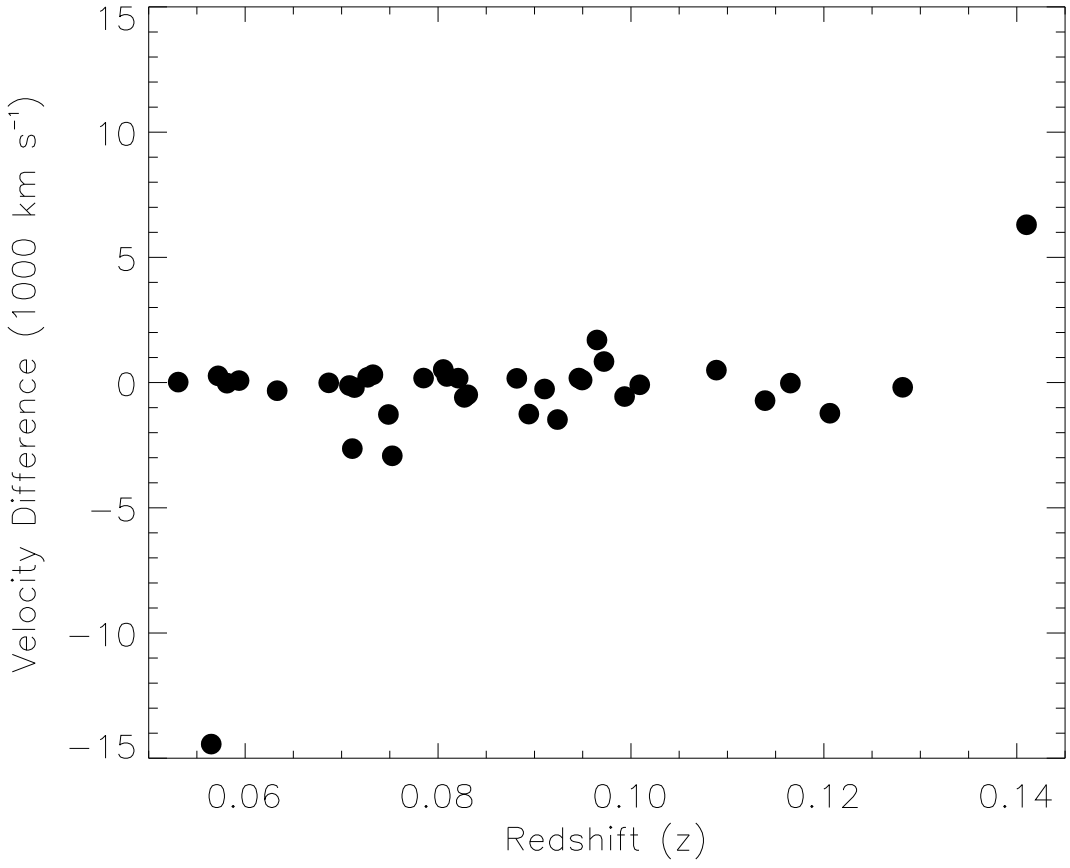

Fig. 1.— The differences for cluster velocities as determined with one measured redshift, compared to velocities determined with an average of nine galaxy redshifts from the MX Survey.

Table 1a. **Results from Other Surveys**

Reference	Clusters	$r_0(h^{-1}Mpc)$	γ
Bahcall & Soneira 1983	104	25.0	-1.8
Ling *et al.* 1986	104	$21.9^{+7.1}_{-5.1}$	-1.7±0.17
Huchra it et al. 1990	145	$20.8^{+6.7}_{-6.9}$	-1.8
West & van der Bergh 1991	64	22.1±6.8	-1.7±0.5
Postman *et al.* 1992	156	$23.7^{+7.9}_{-9.0}$	-1.8±0.2
Peacock & West 1992	195	21.1±1.3	-2.0±0.2
Efstathiou *et al.* 1992	211	14.0 ±1.3	-1.9 ±0.23
Nichol *et al.* 1992	79	16.2 ±2.3	-2.0 ±0.2
Dalton *et al.* 1994	364	14.3 ±2.5	-2.05 ±.12
Nichol *et al.* 1994	67	16.1 ±3.4	-1.9 ±3.4
Abadi *et al.* 1998	248	$21.1^{+1.6}_{-2.3}$	-1.92

Table 1b. **Notes**

Reference	Notes
Bahcall & Soneira 1983	Abell Statistical Sample, R$\geq 1, D \leq 4$
Ling *et al.* 1986	same data as above
Huchra *et al.* 1990	Deep Abell Survey, R≥ 1
West & van der Bergh 1991	cD Abell Clusters
Postman *et al.* 1992	R≥ 1, $m_{10} \leq 16.5$
Peacock & West 1992	Volume limited, R≥ 1
Efstathiou *et al.* 1992	APM[a] $R_{DEMS} \geq 20$
Nichol *et al.* 1992	EDSGC[a] $R_{EDSGC} \geq 22$
Dalton *et al.* 1994	APM[a] $R_{APM} \geq 50$ where $R_{APM} = 24.8 + R_{DEMS}$
Nichol *et al.* 1994	X-ray selected $R \geq 0$ Abell clusters
Abadi *et al.* 1998	X-ray selected $R \geq 0$ Abell clusters

[a]We refer the reader to the individual APM and EDSGC papers for clarification on the richness levels for those catalogs. We simply note here that the clusters in both the APM catalog and the EDSGC catalog are poorer than the $R \geq 1$ Abell clusters.

Table 2. **Results for the Power-Law Fits of ξ**

Sample $m_{10} \leq 16.8, R \geq 1, \lvert b\rvert > 30^\circ$	Size	γ	r_0 (h^{-1}Mpc)
Northern, $\delta \geq -17^\circ$	198	-1.92 ± 0.22	$19.42^{-5.32}_{+4.06}$
Wholesky	289	-1.83 ± 0.15	$23.36^{-4.19}_{+3.66}$
Wholesky, $z < 0.10$	238	-1.88 ± 0.16	$22.79^{-4.58}_{+3.89}$
Wholesky (excluding Cor Bor)	283	-1.85 ± 0.19	$21.36^{-4.13}_{+3.48}$
Wholesky (excluding MSC)	283	-1.94 ± 0.19	$20.42^{-4.46}_{+3.69}$
Wholesky (excluding Ursa Majoris)	285	-1.82 ± 0.16	$22.66^{-4.35}_{+3.77}$
Wholesky (excluding Cor Bor and MSC)	277	-2.13 ± 0.22	$18.38^{-4.13}_{+3.28}$
Wholesky (after rotating Ursa Majoris and Cor Bor)	289	-1.90 ± 0.15	$23.14^{-4.24}_{+3.62}$
Wholesky 19 'contaminated'clusters removed	270	-1.94 ± 0.16	$22.63^{-4.30}_{+3.65}$
Northern cD, Distance $< 350h^{-1}$Mpc $\delta \geq -17^\circ$	104	-1.88 ± 0.47	$20.10^{-11.32}_{+9.86}$

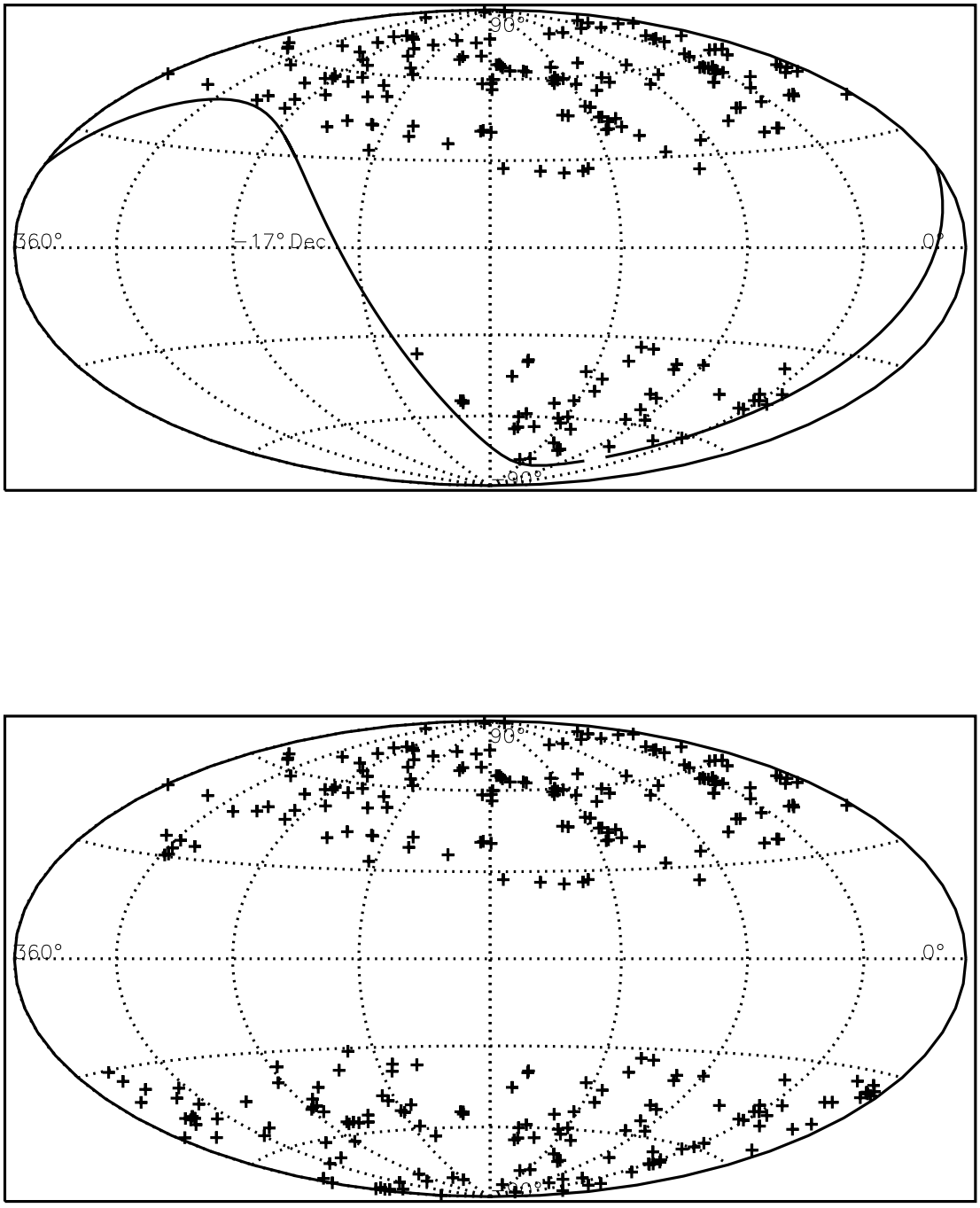

Fig. 2.— **Top:** aitoff projection for the Northern magnitude limited sample of 198 clusters. **Bottom:** Wholesky magnitude limited sample of 198 northern clusters and 91 southern clusters.

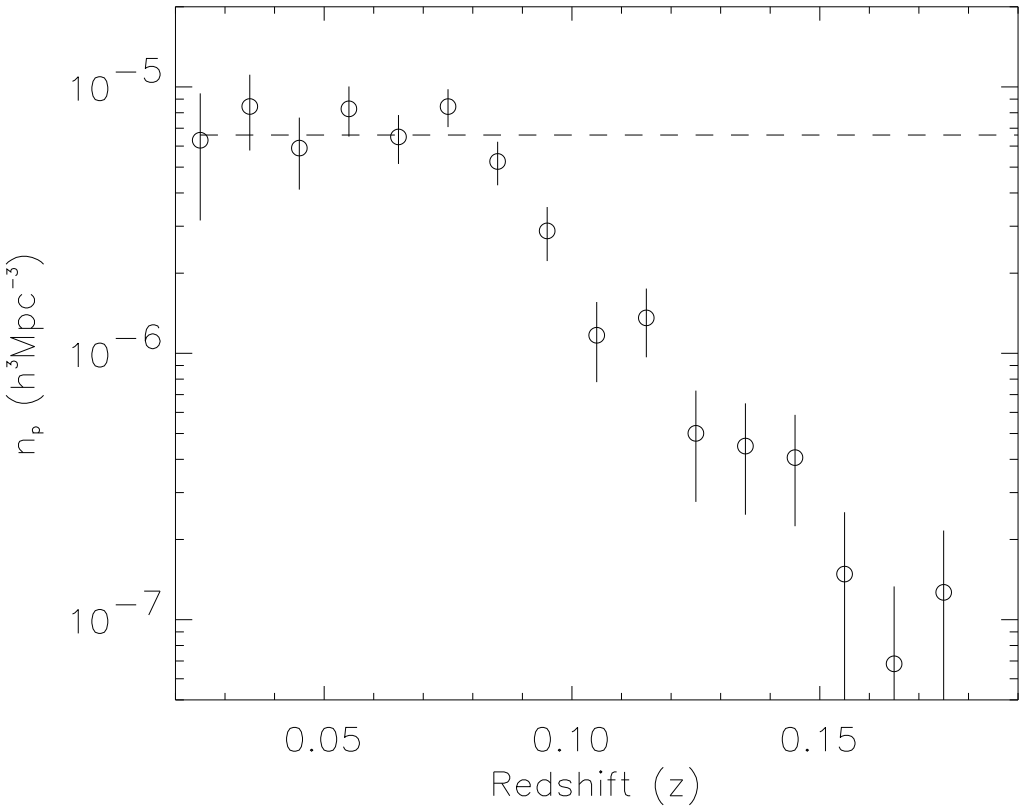

Fig. 3a.— The number density (n_p) for the MX Survey $m_{10} \leq 16.8$ limited sample of $R \geq 1$ clusters. The dashed line is the mean density of $6.60 \times 10^{-6} h^3 \mathrm{Mpc}^{-3}$.

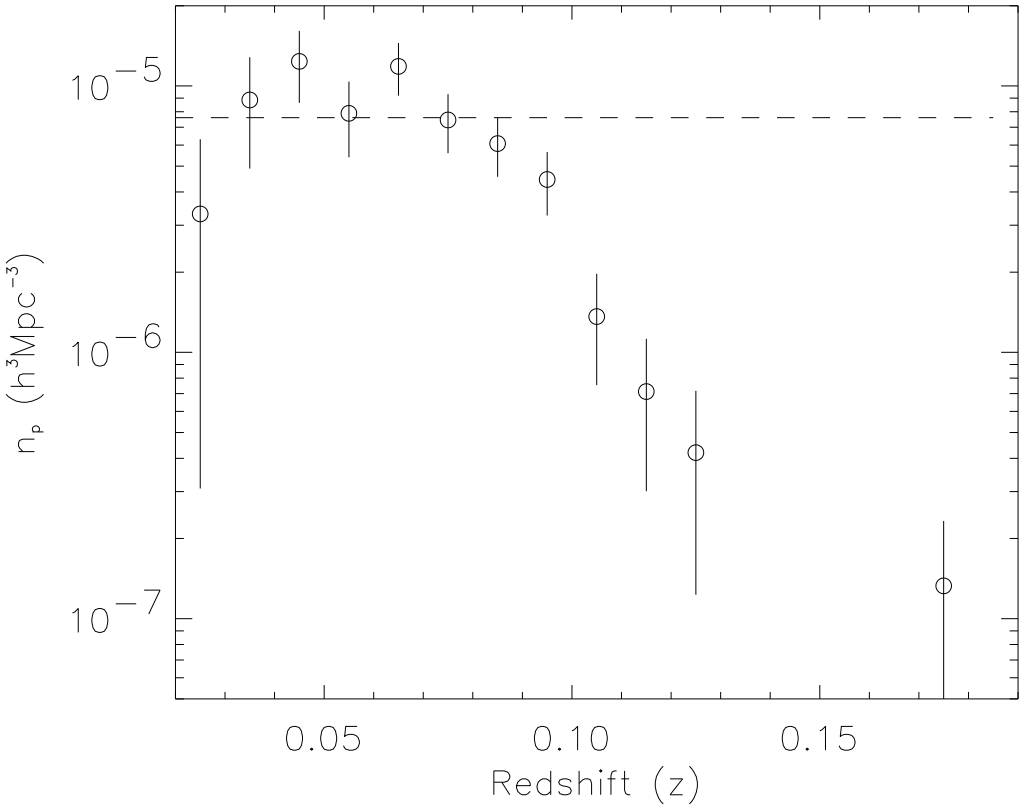

Fig. 3b.— The number density (n_p) for Southern clusters with $m_{10} \leq 16.8$ and $R \geq 1$. The dashed line is the mean density of $7.60 \times 10^{-6} h^3 \mathrm{Mpc}^{-3}$.

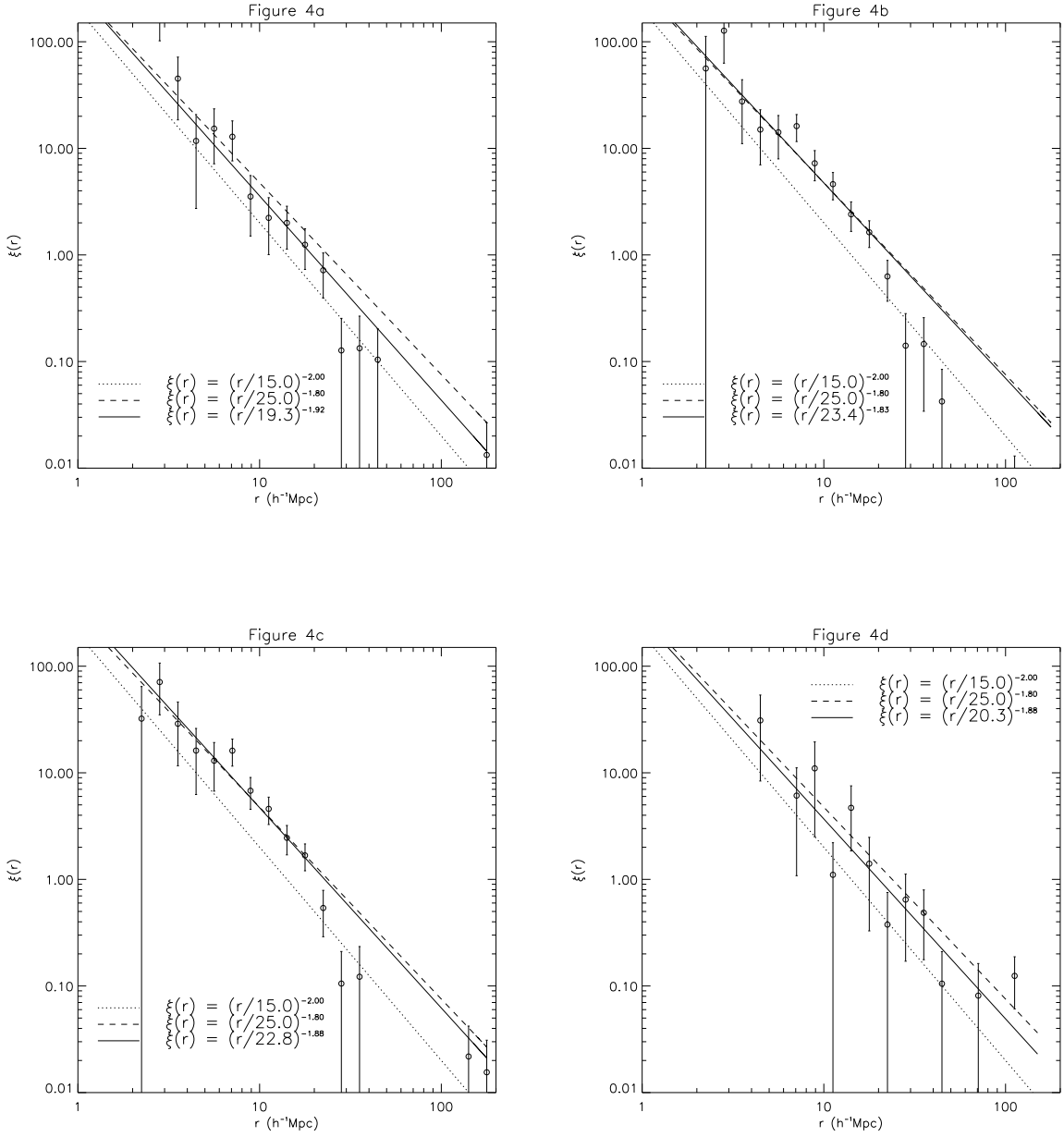

Fig. 4.— **Fig 4a:** The northern magnitude-limited sample of 198 Abell clusters with $m_{10} \leq 16.8$ and $R \geq 1$. **Fig 4b:** The whole-sky magnitude-limited sample of 198 Abell clusters and 91 ACO clusters with $m_{10} \leq 16.8$ and $R \geq 1$. **Fig 4c:** The whole-sky magnitude and volume-limited sample of 158 Abell clusters and 82 ACO clusters with $m_{10} \leq 16.8$, $R \geq 1$ within $286h^{-1}$Mpc ($z = 0.10$). **Fig 4d:** The cD sample of 104 Abell clusters within $350h^{-1}$Mpc.

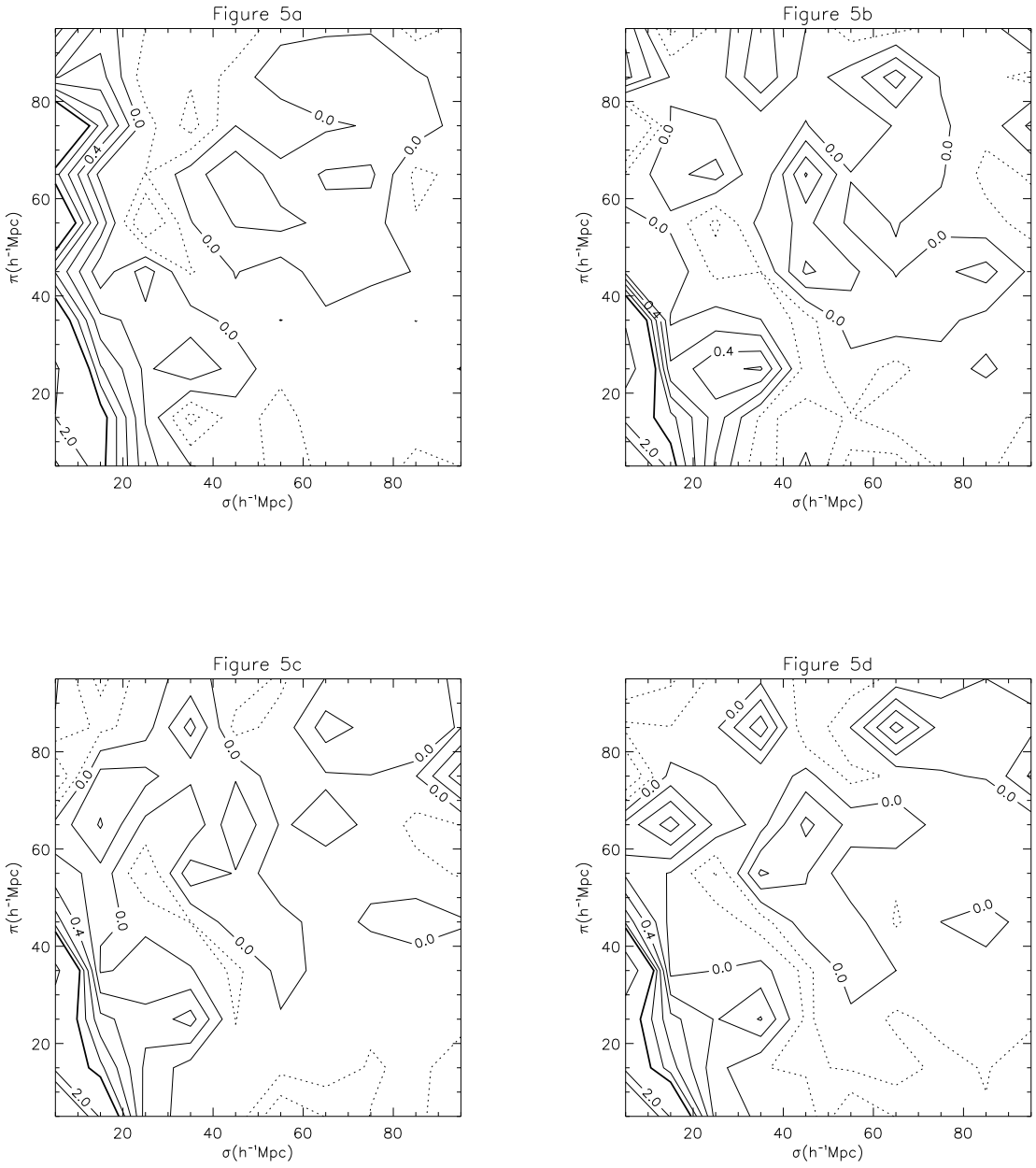

Fig. 5.— **Fig 5a:** The contour plot of $\xi(\sigma, \pi)$ for the original PHG statistical sample of $R \geq 0$, $m_{10} \leq 16.5$, $|b| \leq 30$ Abell clusters. **Fig 5b:** The contour plot of ξ for the MX northern magnitude-limited sample of $R \geq 1$, $m_{10} \leq 16.8$, $|b| \leq 30$ Abell clusters. **Fig 5c:** The contour plot of ξ for the whole-sky magnitude-limited sample of $R \geq 1$, $m_{10} \leq 16.8$, Abell/ACO clusters. **Fig 5d:** The contour plot of ξ for the whole-sky statistical sample.

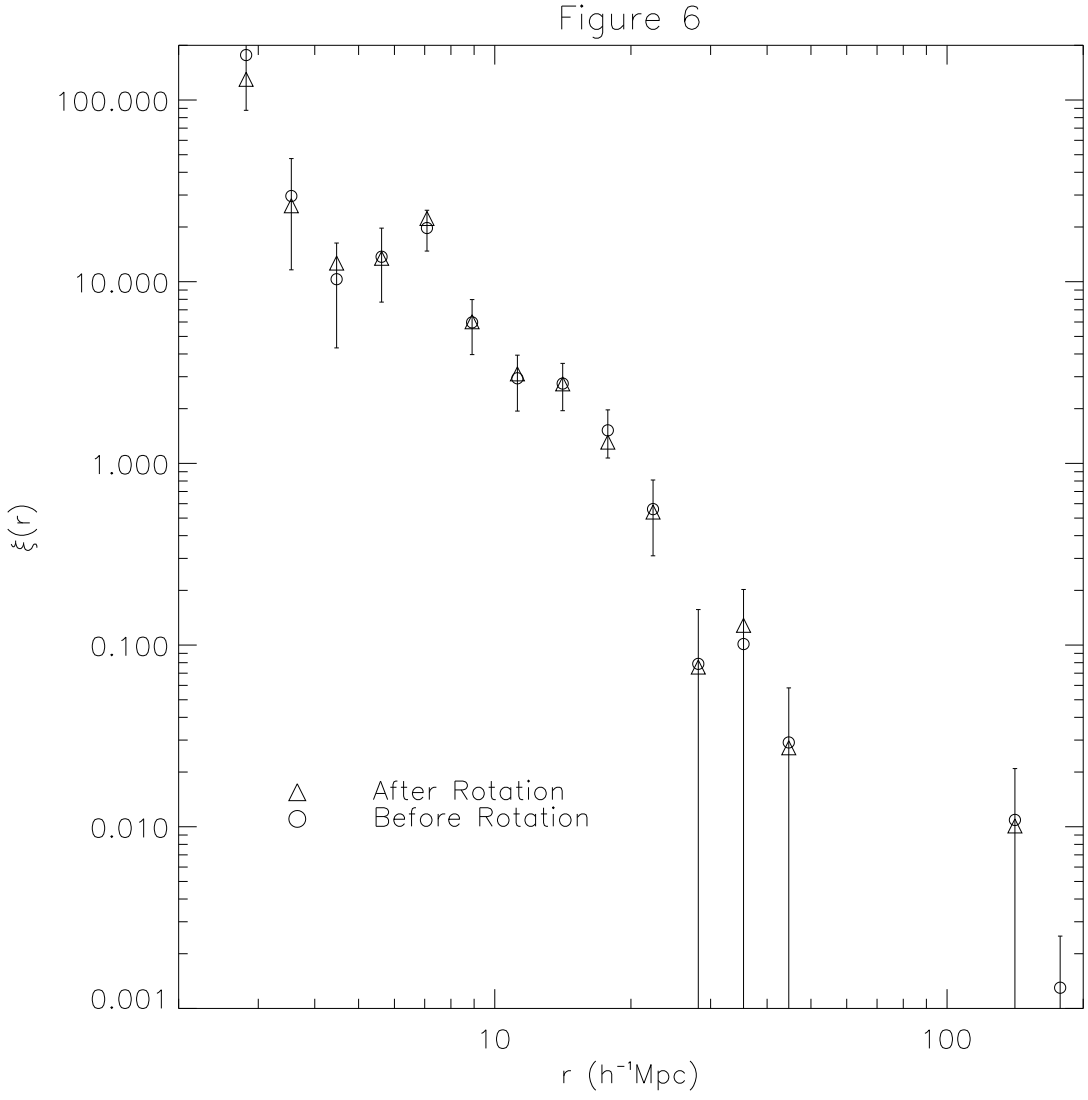

Fig. 6.— $\xi(r)$ for the whole-sky magnitude-limited sample before and after rotating the Ursa Majoris and Corona Borealis superclusters.

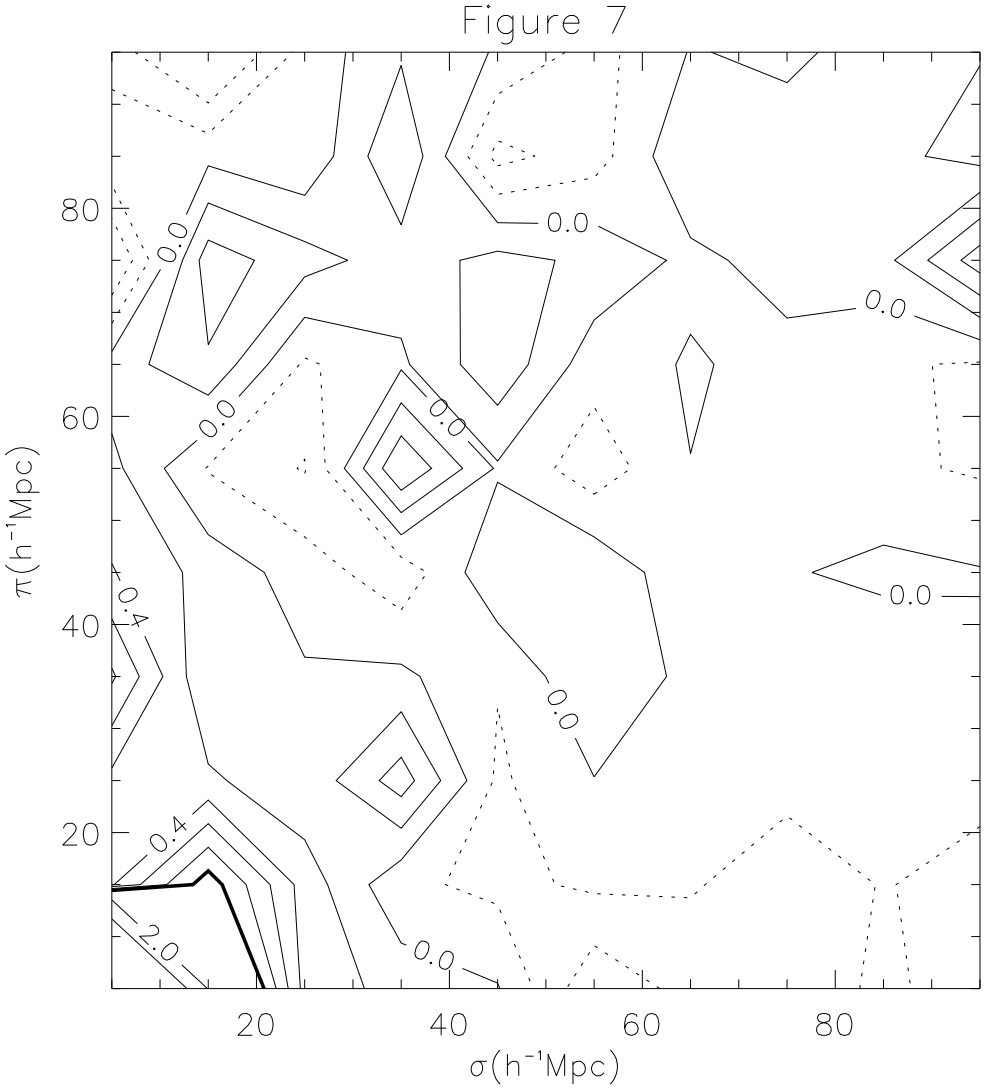

Fig. 7.— $\xi(\sigma, \pi)$ in $10h^{-1}$Mpc bins for the whole-sky magnitude-limited sample after rotating the Ursa Majoris and Corona Borealis superclusters. Compare to Figure 5c.

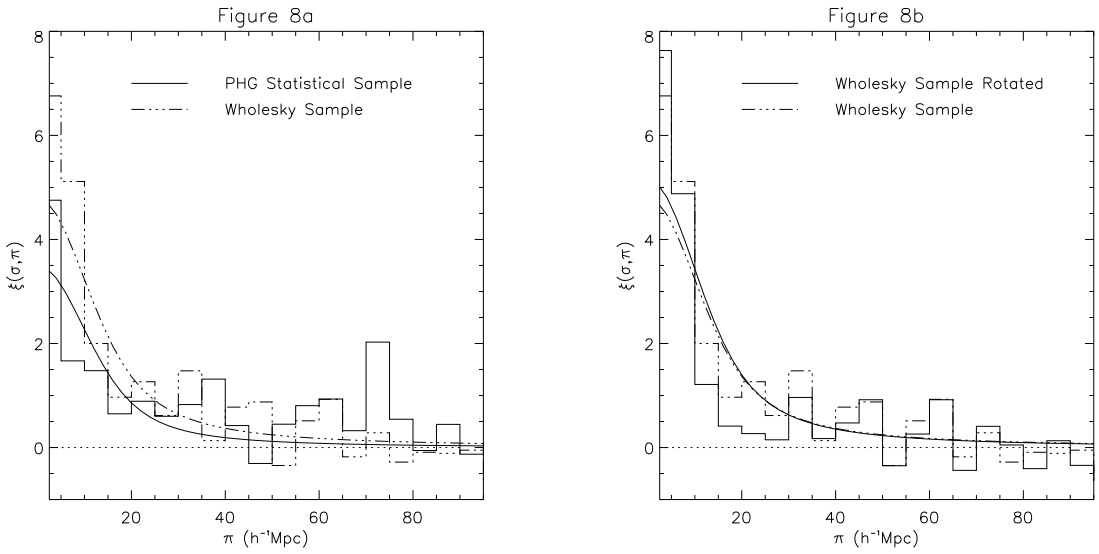

Fig. 8.— **Fig 8a:** $\xi(\sigma, \pi)$ constrained to $0 \leq \sigma \leq 15h^{-1}$Mpc for the PHG statistical sample (solid) and the whole-sky magnitude-limited sample (dash-dot). The smooth line is the respective histogram convolved with a Gaussian of width 700 km s^{-1}. **Fig 8b:** Similar to Fig 8a. The solid line is for the magnitude-limited sample after rotating the Ursa Majoris and Corona Borealis superclusters. The dash-dot line is for before the rotation.

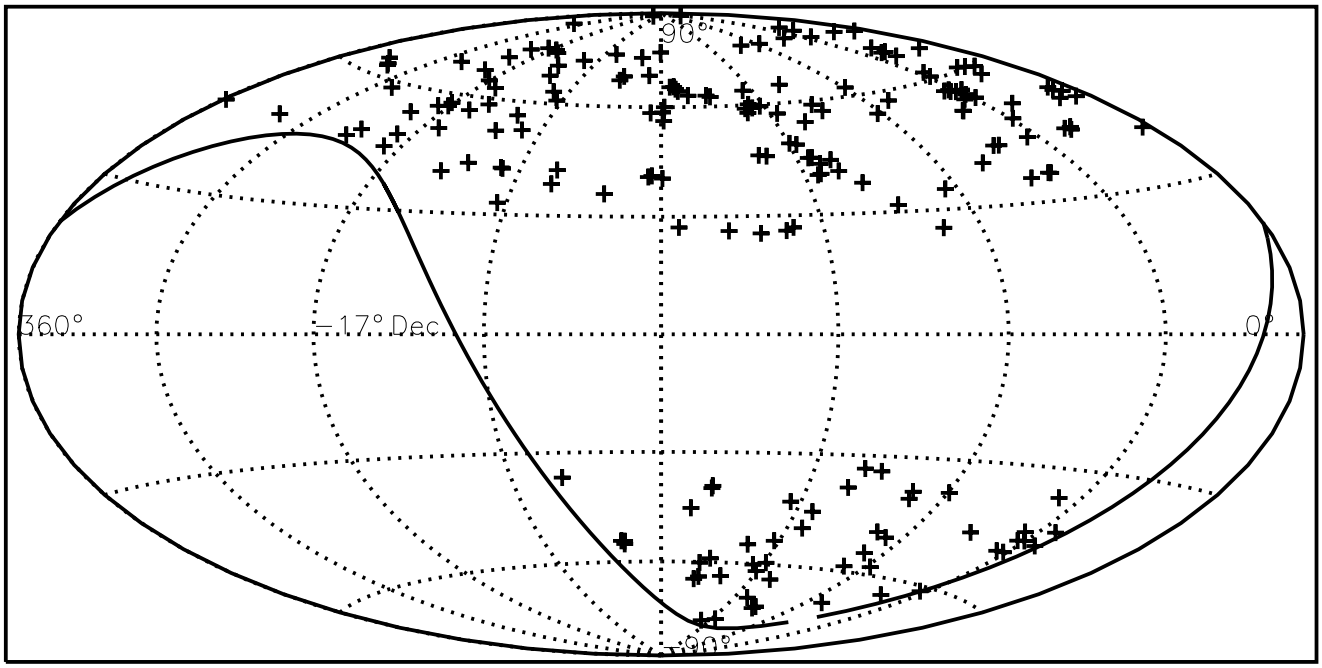
90°
360°
−17° Dec.
0°
−90°

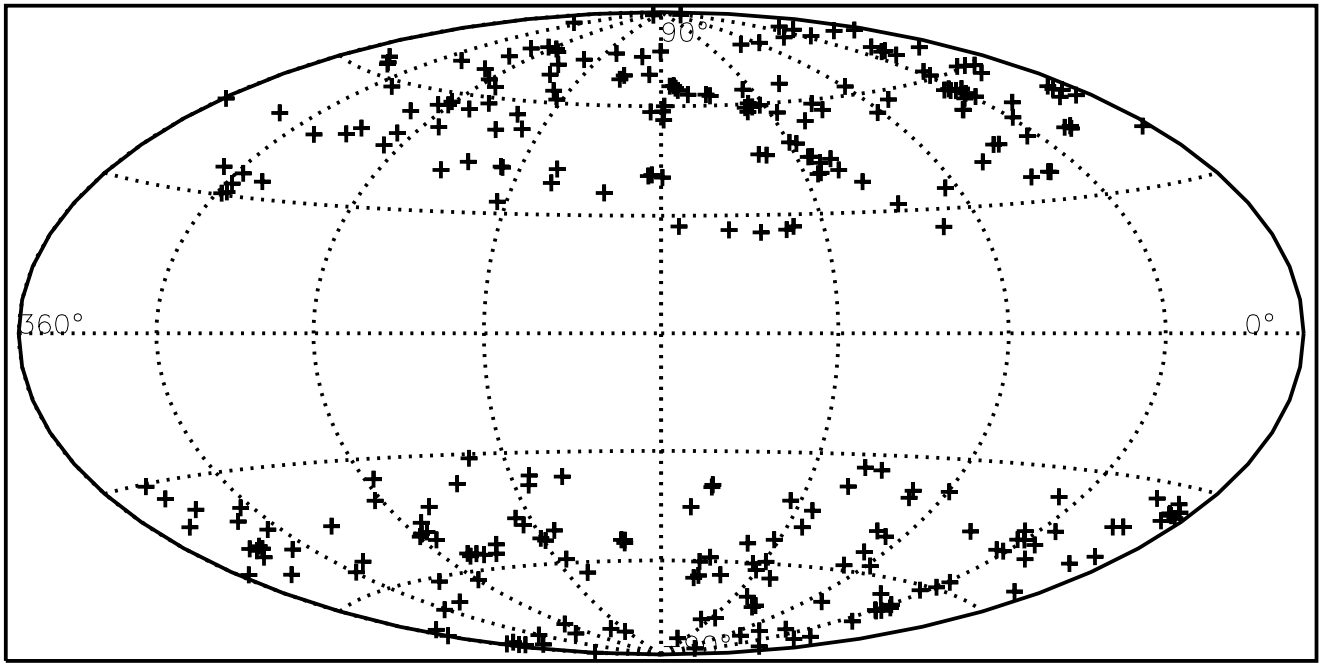
90°
360°
0°
−90°

Figure 5a

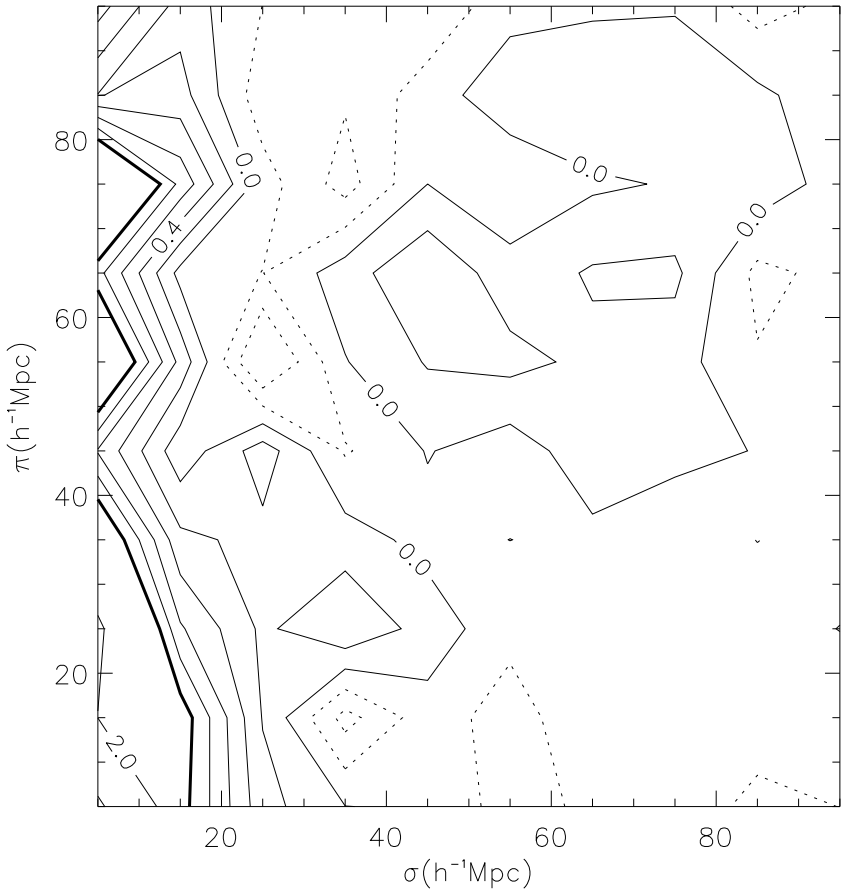

Figure 5b

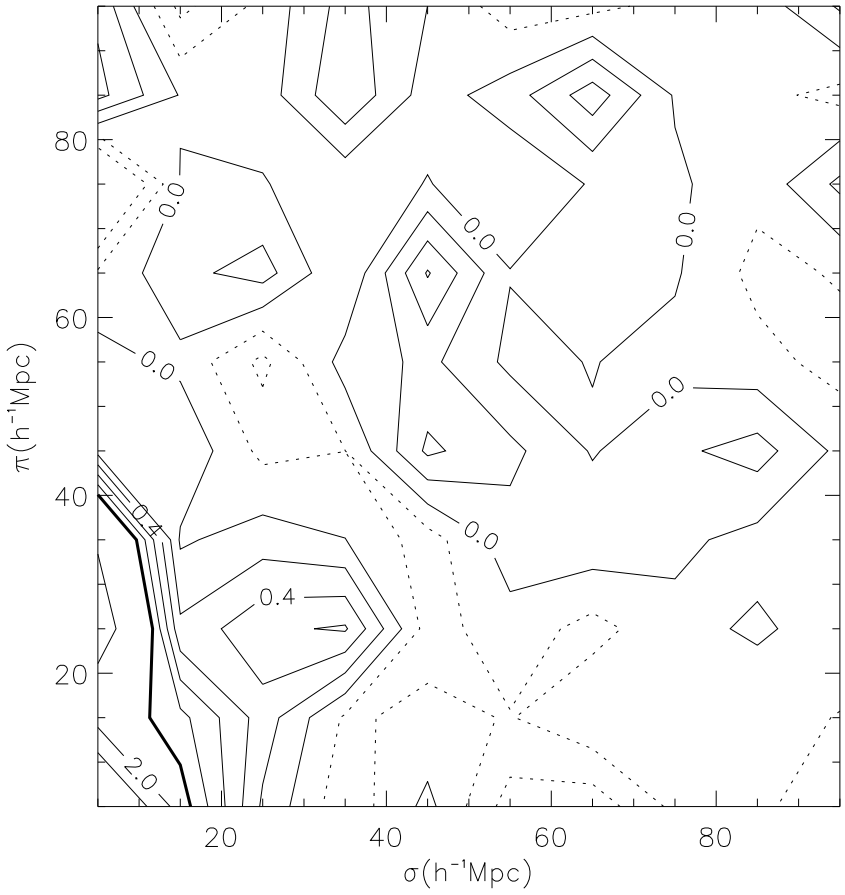

Figure 5c

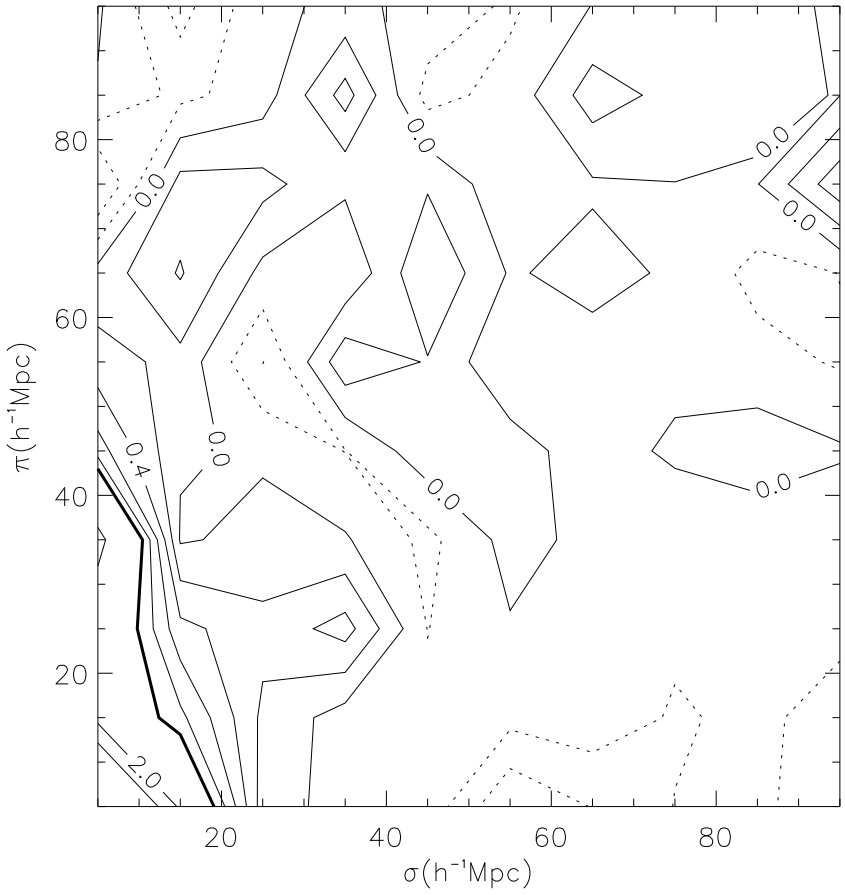

Figure 5d

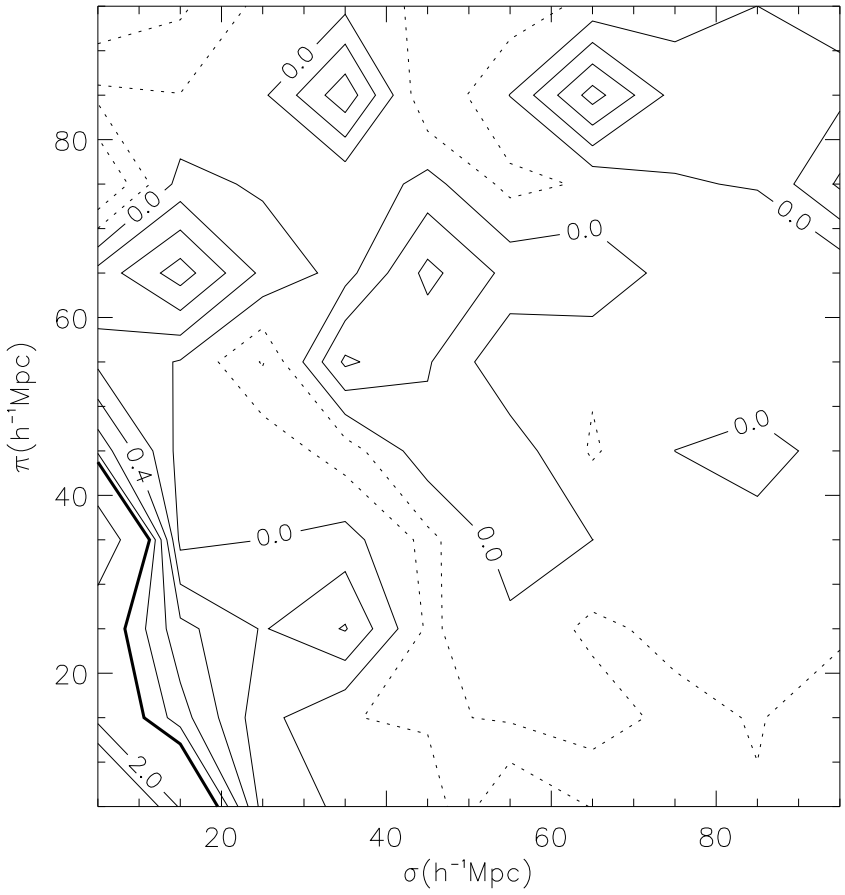

Figure 7

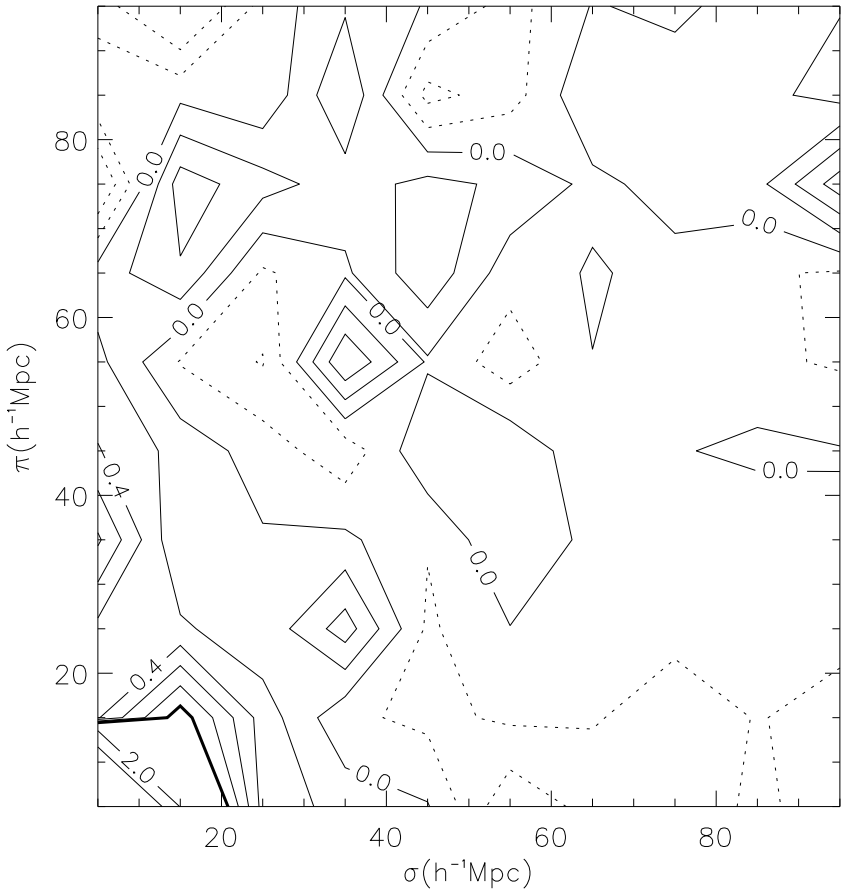

Figure 8a

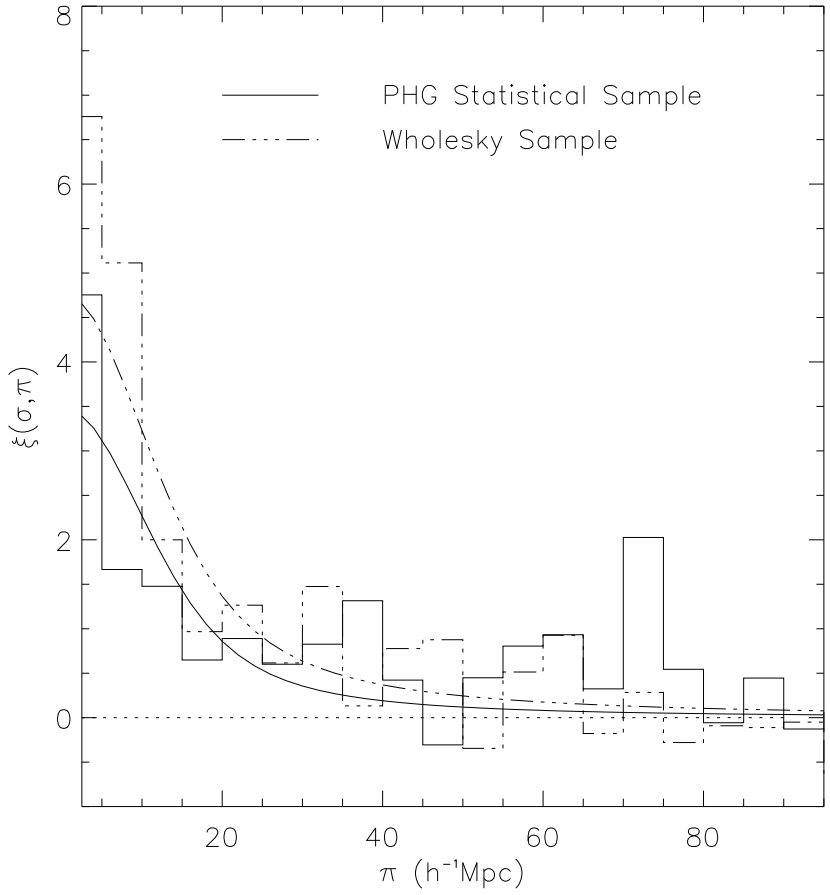
PHG Statistical Sample
Wholesky Sample
8
6
4
2
0
20
40
60
80
$\xi(\sigma,\pi)$
π (h^{-1}Mpc)

Figure 8b

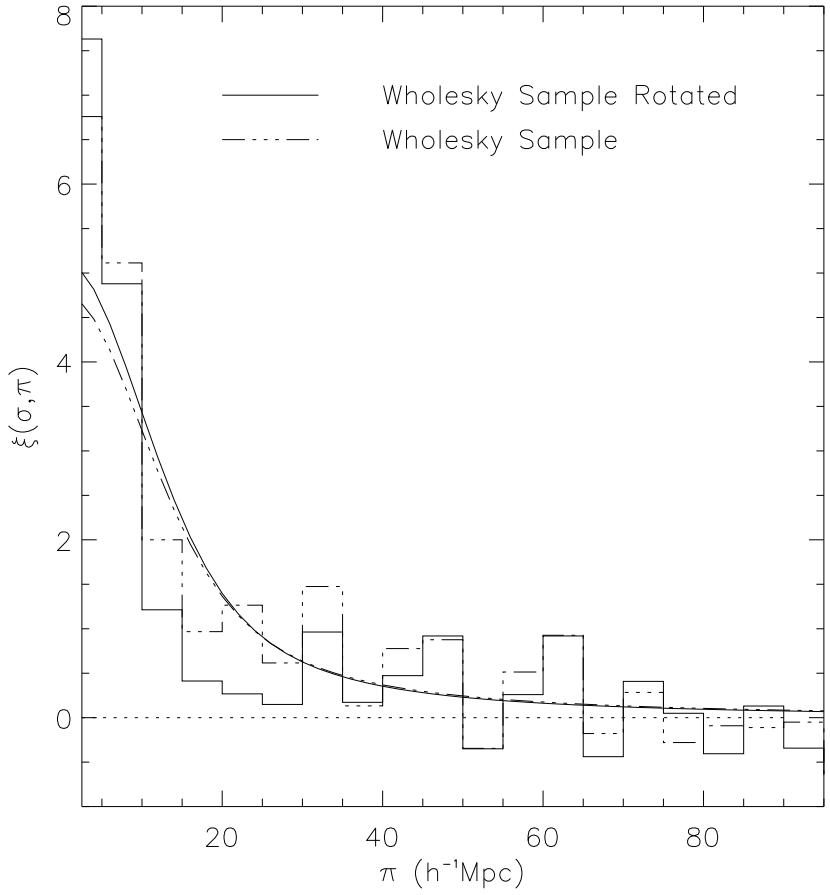
Wholesky Sample Rotated
Wholesky Sample
8
6
4
2
0
20
40
60
80
ξ(σ,π)
π (h⁻¹Mpc)